NAVAL POSTGRADUATE SCHOOL

MONTEREY, CALIFORNIA

THESIS

FREE ELECTRON LASER ANALYSIS FOR THE INNOVATIVE NAVY PROTOTYPE

by

Darin S. Smith

March 2008

Thesis Advisor: William B. Colson
Co-Advisor: Joseph Blau

Approved for public release; distribution is unlimited

THIS PAGE INTENTIONALLY LEFT BLANK

REPORT DOCUMENTATION PAGE			Form Approved OMB No. 0704-0188
Public reporting burden for this collection of information is estimated to average 1 hour per response, including the time for reviewing instruction, searching existing data sources, gathering and maintaining the data needed, and completing and reviewing the collection of information. Send comments regarding this burden estimate or any other aspect of this collection of information, including suggestions for reducing this burden, to Washington headquarters Services, Directorate for Information Operations and Reports, 1215 Jefferson Davis Highway, Suite 1204, Arlington, VA 22202-4302, and to the Office of Management and Budget, Paperwork Reduction Project (0704-0188) Washington DC 20503.			
1. AGENCY USE ONLY ***(Leave blank)***	**2. REPORT DATE** March 2008	**3. REPORT TYPE AND DATES COVERED** Master's Thesis	
4. TITLE AND SUBTITLE Free Electron Laser Analysis For the Innovative Navy Prototype		**5. FUNDING NUMBERS**	
6. AUTHOR(S) Smith, Darin S.			
7. PERFORMING ORGANIZATION NAME(S) AND ADDRESS(ES) Naval Postgraduate School Monterey, CA 93943-5000		**8. PERFORMING ORGANIZATION REPORT NUMBER**	
9. SPONSORING /MONITORING AGENCY NAME(S) AND ADDRESS(ES) N/A		**10. SPONSORING/MONITORING AGENCY REPORT NUMBER**	
11. SUPPLEMENTARY NOTES The views expressed in this thesis are those of the author and do not reflect the official policy or position of the Department of Defense or the U.S. Government.			
12a. DISTRIBUTION / AVAILABILITY STATEMENT Approved for public release; distribution is unlimited		**12b. DISTRIBUTION CODE**	
13. ABSTRACT (maximum 200 words) Free Electron Lasers are the focus of a recently announce Innovative Navy Prototype to develop a directed energy weapon system for the self-defense of ships. Operating in a shipboard environment poses several challenges that must be overcome. Short Rayleigh length systems offer solutions to some of these problems. Simulations were performed to examine the benefit of short Rayleigh length designs in the face of electron beam misalignment. Additionally, simulations were performed to explore the effect of quadrupole misalignment on electron beam position and trajectory, and ultimately on FEL performance.			
14. SUBJECT TERMS Free Electron Laser, FEL, Directed Energy, Quadrupole, Magnet Misalignment			**15. NUMBER OF PAGES** 81
			16. PRICE CODE
17. SECURITY CLASSIFICATION OF REPORT Unclassified	**18. SECURITY CLASSIFICATION OF THIS PAGE** Unclassified	**19. SECURITY CLASSIFICATION OF ABSTRACT** Unclassified	**20. LIMITATION OF ABSTRACT** UU

NSN 7540-01-280-5500 Standard Form 298 (Rev. 2-89)
Prescribed by ANSI Std. 239-18

THIS PAGE INTENTIONALLY LEFT BLANK

Approved for public release; distribution is unlimited

FREE ELECTRON LASER ANALYSIS FOR THE INNOVATIVE NAVY PROTOTYPE

Darin S. Smith
Lieutenant, United States Navy
B.S., Rensselaer Polytechnic Institute, 2000

Submitted in partial fulfillment of the
requirements for the degree of

MASTER OF SCIENCE IN APPLIED PHYSICS

from the

NAVAL POSTGRADUATE SCHOOL
March 2008

Author: Darin S. Smith

Approved by: William B. Colson
Thesis Advisor

Joseph Blau
Co-Advisor

James H. Luscombe
Chairman, Department of Physics

THIS PAGE INTENTIONALLY LEFT BLANK

ABSTRACT

Free Electron Lasers are the focus of a recently announce Innovative Navy Prototype to develop a directed energy weapon system for the self-defense of ships. Operating in a shipboard environment poses several challenges that must be overcome. Short Rayleigh length systems offer solutions to some of these problems. Simulations were performed to examine the benefit of short Rayleigh length designs in the face of electron beam misalignment. Additionally, simulations were performed to explore the effect of quadrupole misalignment on electron beam position and trajectory, and ultimately on FEL performance.

THIS PAGE INTENTIONALLY LEFT BLANK

TABLE OF CONTENTS

LIST OF FIGURES

THIS PAGE INTENTIONALLY LEFT BLANK

LIST OF TABLES

THIS PAGE INTENTIONALLY LEFT BLANK

LIST OF ACRONYMS AND ABBREVIATIONS

ABL	Air Borne Laser
AES	Advanced Energy Systems
cm	Centimeters
COIL	Chemical Oxygen-Iodine Laser
FEL	Free Electron Laser
g	Gram
GHz	Gigahertz
INP	Innovative Navy Prototype
J	Joule
K	Degrees Kelvin
kg	kilogram
kW	kilowatt
Lidar	Light detection and Ranging
linac	Linear accelerator
m	Meter
MIRACL	Mid Infra-Red Advanced Chemical Laser
mm	Millimeters
mrad	Milliradians
MeV	Mega-Electron Volt
MHz	Megahertz
MW	Megawatt
MIRACL	Mid-Infra-Red Advanced Chemical Laser

NPS	Naval Postgraduate School
rad	Radian
RF	Radio Frequency
T	Tesla
THEL	Tactical High Energy Laser
TJNAF	Thomas Jefferson National Accelerator Facility
W	Watts

LIST OF SYMBOLS

a	Dimensionless complex optical field amplitude
A	Area
B	Magnitude of the undulator magnetic field
B_0	Magnetic field of the optical wave
B_M	Magnetic field of the undulator
c	Speed of light
c_Q	Specific heat capacity
e	Electron charge
E	Magnitude of the magnetic and electric fields of the optical wave
E_0	Electric field of the optical wave
G	Optical gain
j	Dimensionless electron beam current
K	Undulator parameter
k	Optical wave number
k_0	Undulator wave number
L	Undulator length
m_e	Electron mass
N	Number of undulator periods
P	Power
R	Radius of curvature
t	time
T	Transfer matrix
Z_0	Rayleigh length
v_z	Electron velocity
β	Dimensionless electron velocity
ε	Emissivity
λ	Optical wavelength
λ_0	Undulator wavelength
ϕ	Initial optical phase
γ	Lorentz factor
ν	Electron phase velocity
ν_0	Initial electron phase velocity
ρ	Electron beam particle density
σ	Stefan Boltzman constant
τ	Dimensionless time
ω_0	Optical frequency
ψ	Optical phase
ζ	Electron phase

THIS PAGE INTENTIONALLY LEFT BLANK

ACKNOWLEDGMENTS

This thesis is not the result of my work alone. Rather it is the culmination of the efforts of many individuals. I wish to gratefully acknowledge the assistance of my advisor, Dr. William Colson, whose patient tutelage provided me with the basic understanding upon which this thesis is founded. I also wish to gratefully acknowledge the assistance of my co-advisor, Dr. Jospeh Blau, who not only provided me with sound advice in writing, but also provided all the tools I needed to complete my simulations.

Thanks to Dr. John Lewellen for sharing his expertise with me. He always managed to tell me exactly what I needed to know in a clear and concise way. Thanks also to Dr. Bob Armstead for serving as a proofreader and providing valuable feedback, and to Eric Adint for fixing the various technical problems that came up

I also wish to thank Dr. Pete Crooker for explaining several basic FEL concepts, as well as spearheading the investigation that inspired the first series of simulations detailed herein, Dave Burggraff whose thesis provided the inspiration for the second series of simulations detailed herein, and for providing me with technical assistance even after he graduated and left.

Finally, I wish to thank my beautiful wife, Victoria, for her loving patience and support. She spent many evenings alone as a thesis widow, but now I am done, and I am coming home.

THIS PAGE INTENTIONALLY LEFT BLANK

I. INTRODUCTION

The United States Navy has a long history of embracing new technologies for the purpose of furthering control of the seas and littoral areas of the world. The Navy is continuing this tradition by funding research for directed energy weapons. High-energy laser systems, which have the potential to fundamentally change the way surface vessels operate, are an important area of this research. A high-energy laser could engage a wide variety of targets, including anti-ship missiles, theater ballistic missiles, aircraft, other surface vessels, and potentially even near-surface mines. Equation Chapter 1 Section 1

High-energy lasers have already been developed and tested for military purposes. A joint US Army and Israeli project has resulted in the development of the tactical high-energy laser (THEL), a mid-infrared advanced chemical laser (MIRACL) that has successfully destroyed Katyusha rockets in flight [1]. The US Air Force has developed a chemical-oxygen-iodine laser (COIL) for use in Air Borne Laser (ABL) program [1]. The US Navy recently approved an Innovative Navy Prototype (INP) to build a Free Electron Laser (FEL) with the goal of reaching the 100 kW power level milestone.

Unlike chemical lasers, an FEL makes use of a relativistic beam of electrons passing through a periodic magnetic field to produce coherent electromagnetic radiation. The components necessary for this method of lasing make FELs larger, heavier, and more expensive than many other lasers used for low power applications. However, the FEL's high power availability and tunable wavelength make it very useful in a wide range of applications at both low and high power. FELs also scale up very favorably, meaning that significantly more powerful FELs need not be very much larger or more costly than lower power versions. Additionally, an FEL is an all-electric system that could run off of ship's power without the need for refueling of dangerous chemicals or explosives, or venting of toxic exhaust fumes. Figure 1 is an illustration of how the Navy might employ an FEL as a weapon system.

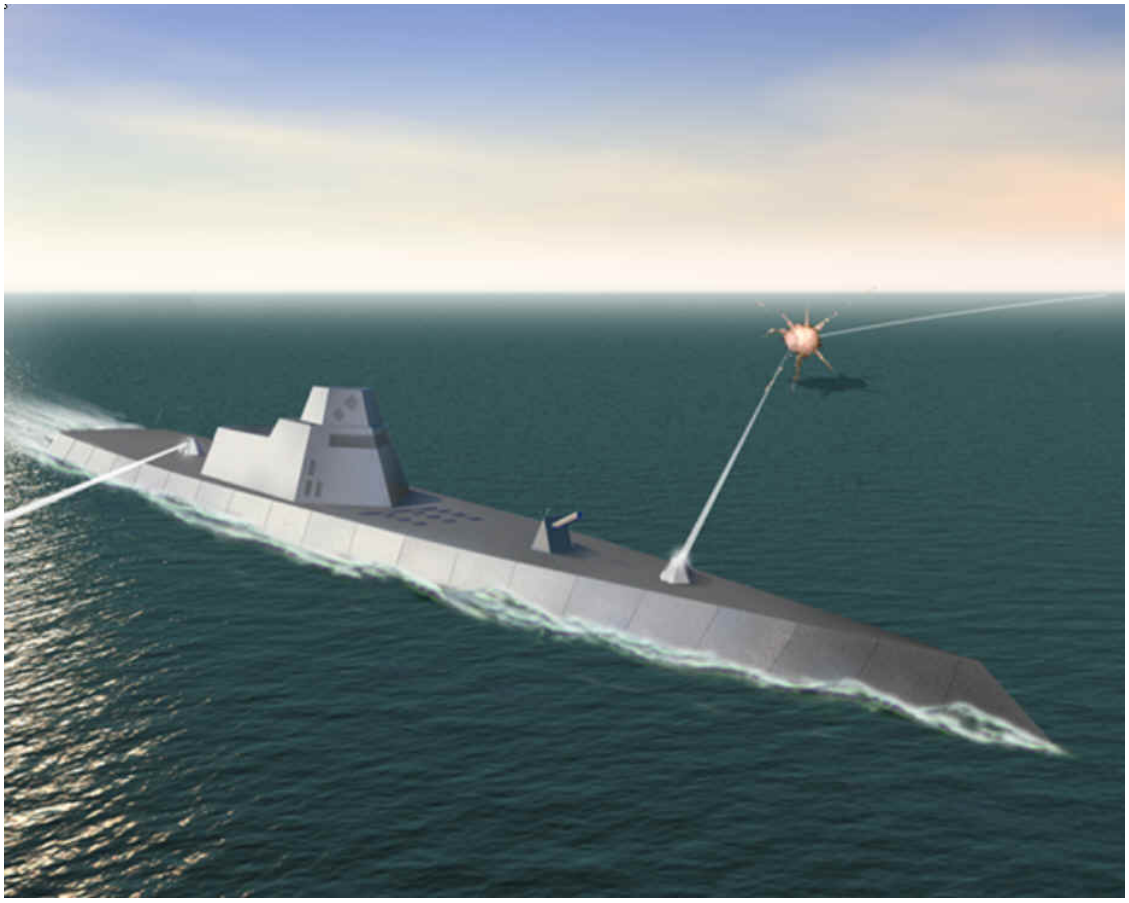

Figure 1. Concept drawing of a shipboard FEL weapon system.

This thesis investigates the effects of quadrupole magnet misalignment on FEL operational performance. This study builds upon work done previously ([2]) to investigate the effects of shifting a single quadrupole, and is aimed at establishing vibration dampening requirements given the effect of shifting multiple quadrupoles. Chapter II provides some background information about the FEL's development and its suitability as a naval weapon system. Chapter III describes the major components of an FEL. Chapter IV discusses the physics of FEL operation. Chapter V describes how the magnetic elements of the electron beam transport system affect electron trajectories. Chapter VI describes simulations that were conducted to determine the affects of quadrupole magnet misalignment. Finally, Chapter VII provides an analysis and summary of the simulations, and suggests directions of further research.

II. BACKGROUND

It is a basic principal of electrodynamics that a charge undergoing an acceleration will radiate electromagnetic waves [3]. This principal often factors into the operation of particle accelerators, which use electric and magnetic fields to accelerate charged particles. The development of particle accelerators, as well as numerous and varied other devices that make use of this principal, is an important part of the history of the FEL. What follows is not an exhaustive history, but rather a broad overview of significant milestones in the development of FELs. First, however, it is instructive to discuss a few related devices. Equation Chapter 2 Section 1

A. RELATED DEVICES

1. Magnetron

Magnetrons are vacuum tubes in which magnetic fields are used to cause electrons from a cathode to spiral around resonator cavities in order to generate coherent microwave radiation. The first magnetron was developed by Albert W. Hull of General Electric in the early 1920's. Magnetrons have been used as amplifiers in radio receivers, and as sources in various radar systems. They are capable of operating at very high efficiency, around 60%. Today they can be found in a wide range of applications, including microwave ovens in the home [4].

2. Cyclotron

Invented in 1929 by Ernest Lawrence of UC Berkley, the cyclotron is a particle accelerator that offered significant advantages over linear accelerators (linacs) previously in use. Accelerators work by using radio frequency (RF) waves to impart energy to charged particles. The size and cost of linacs placed an upper limit on the energies that could practically be achieved. Cyclotrons use a magnetic field to circulate charged particles, making them much smaller and much more efficient then the linear equivalent. The upper limit on energy levels achievable with a cyclotron results from relativistic

effects that cause the particle's mass to increase, which disrupts the particle's orbit and causes it to move out of phase with the RF waves [5].

3. Klystron

The klystron, invented by the brothers Russell and Sigurd Varian of Stanford University in 1937, is a device that uses an evacuated electron tube and two resonant cavities to amplify a reference signal of microwave or radio frequency radiation [6]. Klystrons can be used to produce low power reference signals for radar systems, higher power carrier waves for communications, and very high power driving waves for particle accelerators They can range in frequency from 100's of MHz to 100's of GHz, and produce power levels up to 100's of MW.

4. Synchrotron

The synchrotron was independently invented by Edwin McMillan of UC Berkley and Vladimir I. Veksler of the Soviet Union around the same time in 1945 [5]. It was conceived as a particle accelerator that uses a magnetic field to circulate charged particles, and an electric field to accelerate the particles. The device takes its name from the fact that the electric and magnetic fields must be synchronized with the particle beam. This synchronization takes advantage of a so-called "phase stability" to avoid the problems of a cyclotron at relativistic energies [7]. In addition to accelerating electrons, synchrotrons produce radiation. At first this side effect was considered a nuisance, since it represented an unwanted loss of energy. It has since been recognized that synchrotron radiation possesses some interesting characteristics, such as high polarization, high brilliance, and low emittance. These characteristics make synchrotron radiation useful for a wide range of research and industrial applications [8]. The term synchrotron radiation now applies to all radiation from accelerating charged particles of relativistic energy, whether this takes place in a synchrotron or in some other device.

B. HISTORY OF FEL DEVELOPMENT

Since FELs make use of synchrotron radiation, the first observation of this radiation is a logical place to begin the history of FEL development. This observation was made in 1947 by researchers using a General Electric 70 MeV synchrotron accelerator [9]. The discovery of this radiation was not the goal of the General Electric researchers, nor was it a surprise. The presence of this radiation had already been predicted, and it was speculated that it would place an upper limit on the energy levels attainable by circular accelerators [10].

One of the earliest ancestors of the FEL is described in a 1952 patent by Elmer J. Gorn [11], [12]. The patent, which was submitted in 1947, is for a "Traveling-Wave Electron Reaction Device." The stated purpose of this device was to cause electrons to interact with an electromagnetic wave in such a way as to either give up energy to or extract energy from the wave. In the first case, the device would be an amplifier, and in the second case it would be an electron accelerator. This device was certainly no FEL, as the electron beam was not relativistic, and the emitted light was not very coherent. However, it did employ the concept of an electron-optical wave interaction that relied on a periodicity in the electron beam.

In the 1950's, H. Motz of Stanford University explored the radiation from fast electron beams passing through a series of magnetic fields with alternating polarity, called an undulator [13–16]. It was discovered that undulators could produce synchrotron radiation more efficiently than synchrotron bending magnets could. Using a 3 MeV electron accelerator, Motz produced millimeter wave radiation. Later, using a 100 MeV accelerator he was able to produce visible light. The radiation he produced was not very coherent, though Motz did discuss the possibility that more coherent light might be produced by this method. His work with undulators proved the versatility of this device by demonstrating operation over a range of wavelengths. Undulators are now used in conjunction with storage rings to produce synchrotron radiation for a wide range of research and industrial applications [5].

Another important development, made by R. M. Phillips in the late 1950's, was the ubitron. Somewhat similar to a klystron, this device takes its name from the phrase "undulated beam interaction" [17]. The ubitron produced centimeter and millimeter wavelength radiation at much higher powers than klystrons or magnetrons of the time, and was once evaluated for its potential as a directed energy weapon [11].

The devices described so far either used resonator cavities to produce coherent microwave radiation, or had no resonator mechanism and produced incoherent synchrotron radiation. FELs use either an open resonator or a seed laser to create coherent emission of optical range synchrotron radiation. The first person to demonstrate the operation above threshold of a true FEL was J. H. J. Madey, of Stanford University [18]. In 1977, a free electron laser in oscillator configuration was operated above threshold at a wavelength of 3.4 microns.

C. APPLICATIONS OF A FREE ELECTRON LASER

FELs have a great deal of promise in a wide range of applications. One of the key advantages of an FEL is wavelength "tunability", which makes this type of laser extremely versatile. As will be explained in more detail later, the output wavelength of the laser can be selected in the design process, and can be adjusted even after the system has been constructed.

This "tunability" makes the FEL a good candidate for improving manufacturing in the areas of polymer surface processing, micromachining, and metal surface processing, to name a few [19]. The university of Hawaii is developing an FEL as a light detection and ranging (lidar) transmitter for remote sensing applications [20]. Additionally, FELs offer many advantages in the medical field. Their selectable wavelength would make possible a reduction in scattering, which would improve resolution in imaging applications. It may also be possible to reduce collateral damage in cutting applications by reducing absorption and heating in un-targeted tissues [21].

D. FEL AS A WEAPON

A laser causes damage to a target by delivering a large amount of energy to a small area, causing a portion of the target to reach its melting temperature. Consider a sample of aluminum, 10 cm by 10 cm, and 1 cm thick. Aluminum is a common material in the construction of missiles, and the destruction of this size sample should be enough to cause a missile to break apart in flight [1]. The physical properties of aluminum are summarized in Table 1.

Density	2700 kg/m^3
Thermal conductivity	237 W/m K
Specific heat capacity	900 J/kg K
Melting temperature	933.47 K
Emissivity	0.5
Heat of fusion	11 kJ/mol

Table 1. Physical properties of Aluminum, from [22]

The power radiated away by our heated sample of aluminum is given by

$$P = \varepsilon\sigma A(T_{Al}^4 - T_{env}^4), \tag{2.1}$$

where ε is the emissivity, σ, is the Stefan-Boltzman constant, A is the area, T_{Al} is the temperature of the aluminum and T_{env} is the temperature of the surrounding environment. The power conducted away is given by

$$H = kA(T_{Al} - T_{env}) / \Delta x, \tag{2.2}$$

where k is the thermal conductivity, and Δx is the thickness. Our sample has a surface area of 100 cm^2, and a thickness of 1 cm. Taking T_{env} to be 300 K and T_{Al} to be the melting point of aluminum, (2.1) yields P = 214 W radiated away, while (2.2) yields H = 150 kW conducted through the back of the sample and H = 60 kW conducted through

the edges. The total power leaving our sample of aluminum when it is near its melting point is a little over 200 kW. If more than this amount of power is applied to the sample, the aluminum will melt.

From the density, we find our sample is about 0.3 kg. The heat energy required to bring this amount of aluminum from 300 K up to the melting temperature is given by

$$Q = c_Q m(T_{Al} - T_{env}), \tag{2.3}$$

where c_Q is the specific heat capacity and m is the mass. Substituting from Table 1 results in Q = 175 kJ. One mole of Al is about 27 g, so 0.3 kg is about 11 moles. Using the heat of fusion from Table 1, it takes about 120 kJ to melt this size sample of aluminum. Adding this number to the previously calculated Q, it takes roughly 300 kJ to melt 100 cm^3 of aluminum.

To melt a sample of aluminum, a laser must impart 300 kJ, and do so at a rate greater than 200 kW in order to exceed the cooling by radiation and conduction. A 0.5 MW laser would accomplish this in about 1 second. Leaving room for atmospheric losses as the beam propagates to the target, a FEL needs to be on the order of 1 MW power level to be an effective weapon.

III. FREE ELECTRON LASER COMPONENTS

FELs can be divided into two main categories based on their design; oscillators and amplifiers. As shown in Figure 2, most major components are common to both configurations. In the oscillator configuration, an optical resonator cavity is formed by highly reflective mirrors, similar to traditional molecular lasers. This allows the optical wave to undergo many passes through the undulator, gaining power and inducing stimulated emission. In the amplifier configuration, there is no optical resonator. Instead a seed laser is used to induce stimulated emission. Amplifiers typically have longer undulators then oscillators because the optical wave only has one pass in which to gain power. A third type of FEL is the self-amplified spontaneous emission (SASE) FEL, which is essentially an amplifier with no seed laser.

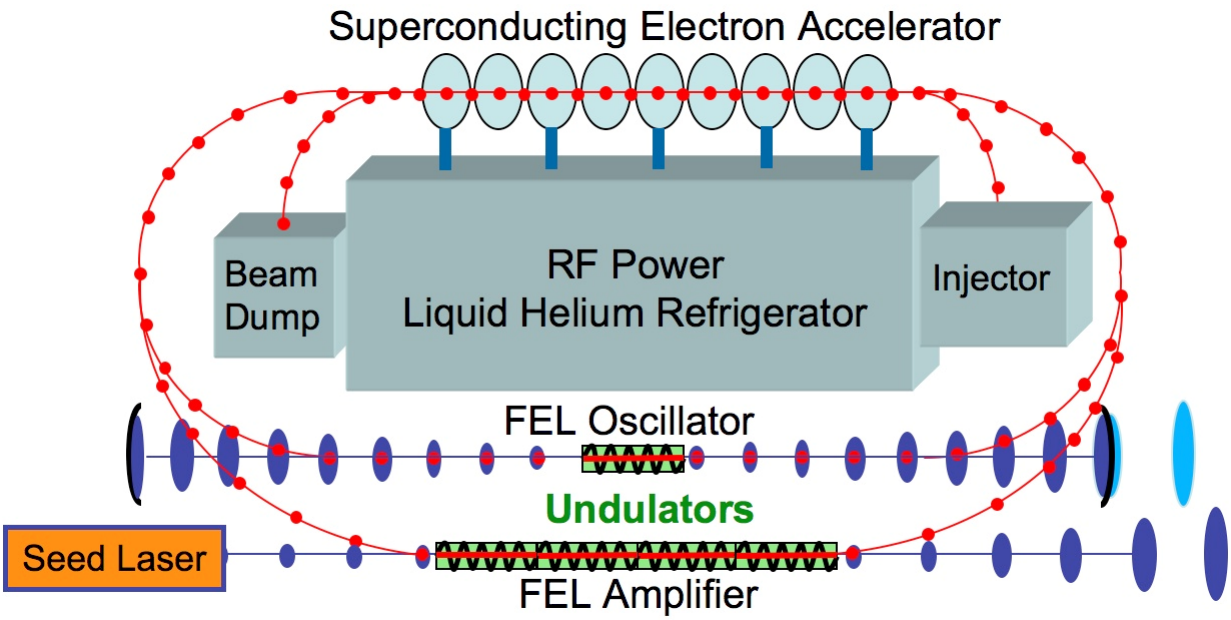

Figure 2. Basic components of a Free Electron Laser, from [1]

A. ELECTRON BEAM COMPONENTS

Before discussing the components related the electron beam, it is instructive to discuss the quality of the electron beam itself. An important measure of electron beam quality is transverse emittance, which is the product of the RMS width and the angular spread of the beam, as measured at the beam waist. Electrons traveling outside of the optical beam will not contribute to the optical gain, so it is desirable to keep the electron beam radius smaller than the waist radius of the optical beam. Another important measure of electron beam quality is energy spread. It is desirable for all of the electrons in a pulse to have very close to the same energy. As will be shown in chapter IV, the energy of the electrons entering the undulator is of critical importance to the operation of the laser. These criteria must be taken into account when considering each of the following components in the electron beam's path.

1. Injector

The injector is where the electron beam originates. There are several ways of producing free electrons, the most common being emission from a photocathode via the photoelectric effect. A drive laser is used to eject electrons from the cathode surface. This drive laser is usually a solid-state pulsed laser, with a pulse rate around 700 MHz. The ejected electrons enter an RF injector that increases their energy to about 5 million electron volts (MeV). This type of injector is well suited for high power FELs because it can produce short electron pulses picoseconds in length, and can produce a high current electron beam of excellent quality.

2. Accelerator

The electron beam from the injector goes directly into the accelerator portion of the laser, where RF energy increases the electron energy from around 5 MeV to around 100 MeV. The accelerator consists of several cavities made of pure niobium, which at temperatures around 2K, becomes superconducting. The alternating RF fields of the cavities are generated by a klystron, and operate at the same frequency as the electron beam injector. The electron pulses coming from the injector are in phase with the RF

fields, so they accelerate as they pass through the cavities. This can also have the effect of shortening the electron pulses, since the slower electrons can be accelerated more than the faster electrons.

After the electrons pass through the undulator, they again pass through the accelerator, this time ~180 degrees out of phase with the RF fields. This causes the electrons to give up most of their energy before going to the beam dump. This second pass through the accelerator reduces cooling and shielding requirements because lower energy electrons produce less heat and radiation upon disposal. Additionally, the energy given up by the electrons during their second pass is effectively recycled, lowering the RF input power required, and increasing the overall efficiency of the system.

3. Undulator

The undulator is contained within the optical resonator cavity, and consists of a series of permanent magnets that set up a magnetic field of alternating polarity. This alternating field is perpendicular to the direction of electron motion, and induces a slight wiggle to the electron's trajectory. For this reason the undulator is sometimes called the "wiggler". As the relativistic electrons oscillate, they emit synchrotron radiation along the axis of the undulator. This emitted radiation amplifies the optical beam already within the resonator cavity. Figure 3 depicts this process.

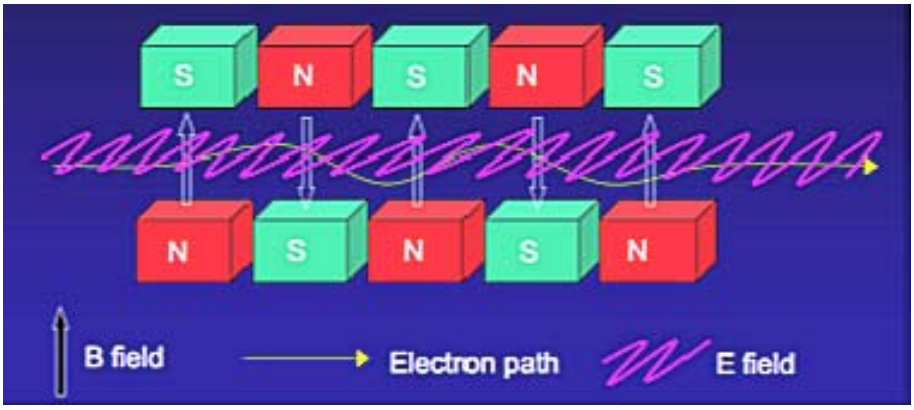

Figure 3. FEL Undulator, from [23]

Undulators may have either linear polarization, as shown in Figure 3, or helical polarization. Linear undulators impart a sinusoidal motion to the electrons, whereas helical undulators impart a corkscrew motion. In either case, the spacing between the magnets is called the undulator period. The undulator period plays a role in determining the frequency of the electron oscillations, and is important in determining the wavelength of the laser.

4. Beam Dump

Since the electron beam quality, which is vital to the operation of the laser, degrades as the electrons pass through the undulator and the turning magnets, the electron beam cannot be used in the undulator a second time. The beam dump is where the electrons end their journey, after passing through the accelerator a second time. The second pass through the accelerator, this time out of phase with the RF field, reduces the electron energy to less than 10 MeV.

The beam dump is essentially a piece of metal, usually aluminum, copper, or tungsten that absorbs the electrons. The beam dump is water cooled to dissipate the heat resulting from the absorption of the electrons.

5. Electron Beam Transport System

Though not pictured in Figure 2, two types of magnets may be found throughout the path of the electron beam. Turning magnets are used to redirect the electron beam so the components discussed above need not all be in a straight line. This allows the whole system to be more compact. They are sometimes referred to as bending magnets or dipole magnets.

Quadrupole magnets are used to focus the electron beam and maintain high beam quality, as discussed at the beginning of this section. There are two types of quadrupole magnets. “F” magnets focus the beam horizontally while defocusing it vertically, while “D” magnets have the opposite effect. How these magnets work will be discussed in more detail in Chapter V.

The path of the electron beam is kept at a vacuum to prevent the electrons from interacting with gas molecules, which would cause an unacceptable reduction in beam energy and quality.

B. OPTICAL BEAM COMPONENTS

1. Optical Resonator Cavity

As mentioned previously, the presence of an optical resonator is the primary difference between oscillator type FELs and amplifier type FELs. In an amplifier, a seed laser synchronized with the pulses of the electron beam is used to initiate the stimulated emission process. The optical beam undergoes significant amplification through the entire length of the undulator, but makes only one pass through. Therefore an amplifier FEL has no optical resonator.

In an oscillator, there is no seed laser. The optical wave is initiated by spontaneous emission from the electrons into the resonator. It then oscillates back and forth through the undulator, acting as the seed for stimulated emission. The mirror on one end of the optical cavity is partially transparent in order to couple the laser light out of the cavity.

Since the optical beam makes many passes through the undulator, the oscillator configuration can use a shorter undulator than the amplifier configuration. This means the overall system can be more compact. This is not without trade-offs, however. First, the distance between the mirrors of the optical cavity must be precisely tuned and maintained so the successive passes of light pulses remain in phase with the electron pulses. Second, if the out-coupling mirror is 50% transparent, then for a megawatt class FEL, the optical beam within the resonator cavity will be several megawatts. If this amount of power is confined within too small of a spot size, then it may destroy the mirrors of the cavity before it could ever be directed toward a target.

2. Beam Director

For an FEL weapon system, the beam director is where the laser light actually leaves the ship to travel to the target. The beam director must be able to aim the beam and track a target. This capability has already been demonstrated, along with the use of adaptive optics to correct for atmospheric turbulence [24].

3. Optical Beam Transport System

The optical beam must be transported from the optical cavity to the beam director. This is accomplished with a series of mirrors, and under vacuum to prevent the beam from losing energy to scattering and absorption. The beam must also be sufficiently large so as not to destroy the mirrors as it makes its way to the beam director, similar to the problem faced within the optical resonator.

C. AUXILIARY SYSTEMS

1. Refrigeration System

As mentioned previously, the accelerator must be kept around 2 K to maintain superconductivity. This can be accomplished with a combination of liquid nitrogen and liquid helium. This cooling system can also provide cooling for the injector, the beam dump, and for the mirrors of the optical resonator cavity.

2. Shielding

The injector, undulator, and beam dump all generate radiation from which humans need to be shielded. Because the electrons are recirculated through the accelerator a second time, their energy level is below the threshold for neutron production (~10 MeV) when they reach the beam dump. This greatly reduces the shielding requirements. However, the electrons entering the beam dump do generate bremsstrahlung radiation. Additionally, synchrotron radiation is generated at the bending

magnets where the electron beam direction is altered. The radioactivity decays very rapidly once the system is shut down, but some shielding is required to protect personnel from radiation hazards during laser operation.

3. Vibration Control

As mentioned previously, mirror spacing and alignment is crucial to FEL operation. Vibrations normally found in a shipboard environment could interfere not only with mirror alignment, but also with the alignment of the quadrupole magnets. Vibration isolation mounting, and an active alignment system will be required to ensure proper operation.

THIS PAGE INTENTIONALLY LEFT BLANK

IV. BASIC PHYSICS OF FREE ELECTRON LASER OPERATION

A. ELECTRON BEHAVIOR

In the following sections, the z-axis will denote the longitudinal axis, passing through the center of the undulator. Electron velocities will usually be normalized to the speed of light as follows: Equation Chapter 4 Section 1

$$\beta_x \equiv v_x / c$$
$$\beta_y \equiv v_y / c$$
$$\beta_z \equiv v_z / c$$
$$\vec{\beta} \equiv \left(\beta_x, \beta_y, \beta_z\right)$$

The undulator period is λ_0.

1. Undulator Fields and Electron Motion

To first order approximation, electrons travel straight through the undulator, down the z-axis at very near the speed of light

$$z(t) = v_z t = \beta_z c t \approx c t. \tag{4.1}$$

However, there is a more subtle motion undergone by the electrons due to the fields that are present. Inside the undulator, the electrons are exposed to three fields; the magnetic field from the undulator magnets, and the magnetic and electric fields of the optical wave. The magnetic field from the magnets of a helical undulator is

$$\vec{B}_M = B\left(\cos(k_0 z), \sin(k_0 z), 0\right), \tag{4.2}$$

where $k_0 = 2\pi/\lambda_0$ is the undulator wave number. The electric and magnetic fields from a corresponding circularly polarized optical plane wave are

$$\vec{E}_0 = E\left(\cos\psi, -\sin\psi, 0\right), \tag{4.3}$$
$$\vec{B}_0 = E\left(\sin\psi, \cos\psi, 0\right), \tag{4.4}$$

where $\psi = kz - \omega t + \phi$, ω is the optical frequency, ϕ is the optical phase, and $k = 2\pi/\lambda$ is the optical wave number.

Electron motion in the presence of these fields can be determined using the relativistic Lorentz force equations,

$$\frac{d(\gamma\vec{\beta})}{dt} = -\frac{e}{m_e c}(\vec{E} + \vec{\beta} \times \vec{B}), \tag{4.5}$$

$$\frac{d\gamma}{dt} = -\frac{e}{m_e c}\vec{\beta} \cdot \vec{E}, \tag{4.6}$$

$$\gamma = \frac{1}{\sqrt{1-\beta^2}}, \tag{4.7}$$

Where e is the electron charge magnitude, m_e is the electron mass, and γ is the Lorentz factor. Substituting the field equations (4.2, 4.3, and 4.4) into the Lorentz force equation (4.5) results in the following equations of electron motion,

$$\frac{d(\gamma\beta_x)}{dt} = -\frac{e}{m_e c}[E\cos\psi(1-\beta_z) - \beta_z B\sin(k_0 z)], \tag{4.8}$$

$$\frac{d(\gamma\beta_y)}{dt} = -\frac{e}{m_e c}[-E\sin\psi(1-\beta_z) + \beta_z B\cos(k_0 z)], \tag{4.9}$$

$$\frac{d(\gamma\beta_z)}{dt} = -\frac{e}{m_e c}[E(\beta_x\cos(\psi) - \beta_y\sin(\psi)) + B(\beta_x\sin(k_0 z) - \beta_y\cos(k_0 z)]. \tag{4.10}$$

Since the electrons are traveling close to the speed of light, $\beta_z \approx 1$, so that (1-β_z) is very small. Therefore the first term inside the brackets in (4.8) and (4.9) can be neglected. Physically, this means the electrons are traveling so fast that the influence of the optical wave's electric field on electron transverse trajectories is negligible compared to the influence of the undulator. Equations (4.8) and (4.9) can then be integrated with respect to time to produce

$$\beta_x = -\frac{K}{\gamma}\cos(k_0 z), \tag{4.11}$$

$$\beta_y = -\frac{K}{\gamma}\sin(k_0 z), \tag{4.12}$$

where K is the dimensionless undulator parameter, defined as $K \equiv eB\lambda_0 / 2\pi m_e c^2$. The constants of integration have been taken to be zero, corresponding to perfect injection of the electrons into the helical undulator. Noting that $k_0 z \approx k_0 ct = \omega_0 t$, (4.11) and (4.12) can be integrated to obtain

$$x(t) = \frac{-Kc}{\omega_0 \gamma} \sin(\omega_0 t) = \frac{-K\lambda_0}{2\pi\gamma} \sin(\omega_0 t), \tag{4.13}$$

$$y(t) = \frac{Kc}{\omega_0 \gamma} \cos(\omega_0 t) = \frac{K\lambda_0}{2\pi\gamma} \cos(\omega_0 t), \tag{4.14}$$

which gives the trajectory of the electrons in the x and y directions. In a helical undulator, the motion of the electrons resembles a corkscrew. It is instructive to use some typical values to put this corkscrew motion into perspective. Typically, $K \sim 1$, $\gamma \sim 100$, and $\lambda_0 \sim 5\,\text{cm}$. This gives oscillations in the x and y directions on the order of 80 microns, which is almost half of a typical electron beam waist diameter of 200 microns. The frequency of these oscillations is $\omega_0/2\pi = c/\lambda_0 = 6\,\text{GHz}$. The electrons are oscillating at microwave frequencies, but the laser operates at infrared frequencies due to relativistic Doppler shifts [1].

2. Microscopic Electron Motion and the Pendulum Equation

The longitudinal motion of the electrons is very straightforward, as described by (4.1). In the previous section, the transverse motion of the electrons was examined on a scale where the effects of the optical wave fields were considered negligible. Now we will investigate electron motion on an even smaller scale, where it will be shown that the effects of the optical wave fields, while small in magnitude, are vital to understanding FEL operation.

Substituting (4.11) and (4.12) into (4.10) gives us

$$\frac{d(\gamma\beta_z)}{dt} = -\frac{e}{m_e c}\left[\begin{array}{l} E\left(-\frac{K}{\gamma}\cos k_0 z \cos\psi + \frac{K}{\gamma}\sin k_0 x \sin\psi\right) \\ +B\left(-\frac{K}{\gamma}\cos k_0 z \sin k_0 z + \frac{K}{\gamma}\sin k_0 z \cos k_0 z\right) \end{array}\right], \tag{4.15}$$

$$\dot{\gamma}\beta_z + \gamma\dot{\beta}_z = \frac{eKE}{\gamma m_e c}\left(\cos k_0 z \cos\psi + \sin k_0 x \sin\psi\right), \tag{4.16}$$

$$\gamma\dot{\beta}_z = \frac{eKE}{\gamma m_e c}\cos\left(k_0 z + \psi\right) - \dot{\gamma}\beta_z\,. \tag{4.17}$$

We can also substitute (4.11) and (4.12) into (4.6) to get

$$\frac{d\gamma}{dt} = \dot{\gamma} = \frac{eKE}{\gamma m_e c}\cos\left(k_0 z + \psi\right). \tag{4.18}$$

If (4.18) is then substituted into (4.17), we get

$$\dot{\beta}_z = (1-\beta_z)\frac{eKE}{\gamma^2 m_e c}\cos\left(k_0 z + \psi\right). \tag{4.19}$$

At this point it is useful to introduce the electron phase, $\zeta = (k + k_0)z - \omega t$. Since k, k_0, and ω are fixed, ζ follows the electron's position in z. The electron phase may be interpreted as a measure of the electron's position relative to the optical wave. It is this relative position that determines whether the electron gives energy to the optical wave, or vice versa. Taking the first and second derivatives with respect to time of the electron phase, we get

$$\dot{\zeta} = (k + k_0)\beta_z c - \omega, \tag{4.20}$$

$$\ddot{\zeta} = (k + k_0)c\dot{\beta}_z. \tag{4.21}$$

Solving for β_z and $\dot{\beta}_z$ we get

$$\beta_z = \frac{\dot{\zeta} + \omega}{(k + k_0)c}, \tag{4.22}$$

$$\dot{\beta}_z = \frac{\ddot{\zeta}}{(k + k_0)c}. \tag{4.23}$$

Since $\lambda \ll \lambda_0$, it follows that $k \gg k_0$. Also, since $\beta_z \approx 1$ and $\omega = kc$, we see from (4.22) that $\dot{\zeta} \ll \omega$. So (4.22) can then be simplified to

$$\beta_z = \frac{\omega}{(k + k_0)c}. \tag{4.24}$$

Substituting (4.23) and (4.24) into (4.19)

$$\frac{\ddot{\zeta}}{(k + k_0)c} = \left(1 - \frac{\omega}{(k + k_0)c}\right)\frac{eKE}{\gamma^2 m_e c}\cos\left(\zeta + \phi\right),$$

$$\ddot{\zeta} = \frac{eKE}{\gamma^2 m_e c}\left[\left(k + k_0\right)c - \omega\right]\cos\left(\zeta + \phi\right),$$

$$\ddot{\zeta} = \frac{eKEk_0}{\gamma^2 m_e}\cos\left(\zeta + \phi\right). \tag{4.25}$$

Before proceeding, it will be useful to normalize our parameters to the dimensions of the undulator. If there are N periods in the undulator, then the undulator length is $L = N\lambda_0$, and we can introduce the dimensionless time parameter $\tau \equiv ct / L$. As the optical wave makes a single pass through the undulator, τ goes from 0 to 1. Derivatives may now be taken with respect to τ rather than t, and denoted as $\overset{o}{(..)} = d(..)/d\tau$ rather than $\overset{\bullet}{(..)} = d(..)/dt$.

It is also convenient to combine the constants in front of the cosine term in (4.25) to introduce the dimensionless optical field magnitude

$$|a| = \frac{2\pi NeKEL}{\gamma^2 m_e c^2}. \tag{4.26}$$

With these simplifications, (4.25) may now be written as

$$\overset{oo}{\zeta} = \overset{o}{\nu} = |a|\cos(\zeta + \phi), \tag{4.27}$$

where $\nu = \overset{o}{\zeta}$ is the electron phase velocity.

Equation (4.27) is in the form of the well-known pendulum equation, and describes the microscopic behavior of the electrons within an optical wavelength. The behavior of simple pendulums is well understood, and can be easily explained with the use of phase space diagrams. Likewise, (4.27) allows the evolution of electrons within the undulator to be demonstrated with phase space diagrams.

3. Phase Space Evolution, Resonance, and Bunching

The meaning of electron phase was described above. Equation (4.27) describes how the electron phase velocity changes with time. Changes in electron phase velocity result from exchanges of energy between the electrons and the optical wave [25]. The electron phase velocity increases when the electron gains energy, and decreases when the electron loses energy. If there is no energy exchange, the electron phase remains constant and the electron phase velocity is zero. The mechanical analog of this is a motionless pendulum at the bottom of its arc, with no exchange between kinetic and potential energy. Recalling that $\omega = kc$, we can set (4.20) equal to zero and solve to find

$$\lambda = \lambda_0 \frac{1-\beta_z}{\beta_z}, \tag{4.28}$$

which is known as the resonance condition. Note that the optical wavelength, λ, depends upon the undulator wavelength, λ_0. This is one of the features that make an FEL "tunable." If we replace β_z with v_z/c in (4.28), then we see

$$\lambda = \lambda_0 \frac{1-v_z/c}{v_z/c} = \lambda_0 \frac{c-v_z}{v_z} = \lambda_0 \left(c/v_z - 1\right),$$
$$\frac{\lambda + \lambda_0}{c} = \frac{\lambda_0}{v_z}. \tag{4.29}$$

The right hand side of (4.29) is simply the amount of time required for an electron to pass through one undulator wavelength. At resonance, this is equal to the amount of time required for the optical wave to travel one optical wavelength further. In other words, at resonance the optical wave outruns the electron by a distance of one optical wavelength. Figure 4 illustrates this concept. The red circle represents a single electron as it travels from left to right. The undulator wavelength is shown in green, and the optical wave is shown in blue.

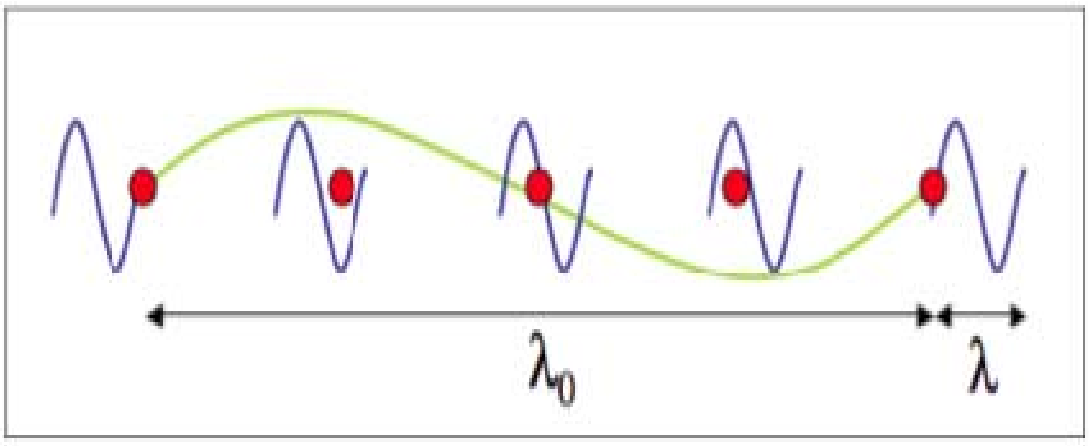

Figure 4. Electron in resonance condition, from [1]

Figure 5 depicts the evolution in phase space of 20 sample electrons as they pass through the undulator from left to right. The electrons, shown as red dots, begin with zero initial phase velocity, in other words on resonance, but evenly distributed in phase. In the phase space diagrams, the vertical axis is phase velocity, which corresponds to

electron energy. The horizontal axis is electron phase, which represents electron position relative to the optical wave. The "lemon-shaped" curve represents the separatrix, which carries the same meaning here as it would in a phase space plot of pendulum motion, with paths inside representing closed orbits and paths outside representing open orbits. In this case, all electrons are following closed orbits. Note that at the end of the undulator, half of the electrons have decreased in phase velocity, meaning energy was transferred to the optical wave, and half have increased in phase velocity, meaning energy was taken away from the optical wave. At resonance there is no net optical gain.

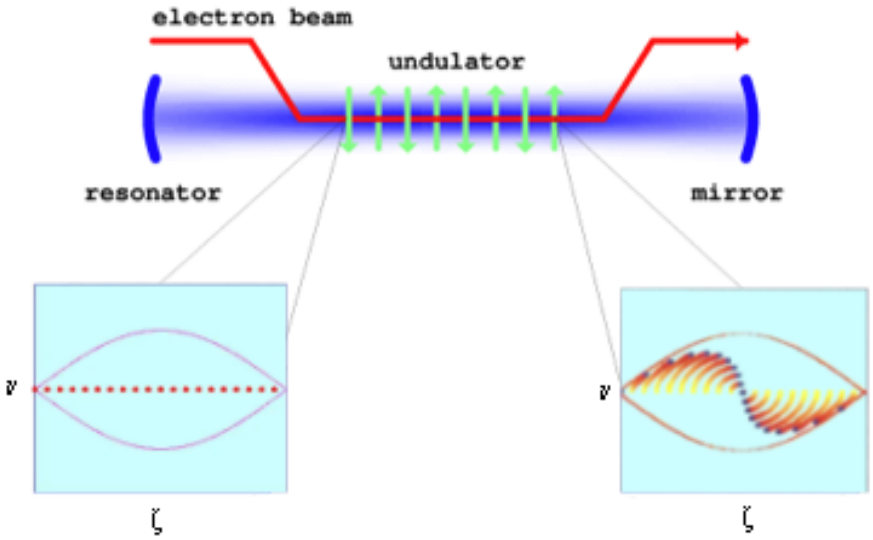

Figure 5. Phase space evolution at resonance, from [1].

Also worth noting is the bunching effect. When entering the undulator, the electrons are uniformly distributed in phase. By the end of the undulator, the electrons have bunched around a specific value of phase. The reason for this can be understood by examining (4.27). Electrons with phases in the range $-\pi/2 < \zeta + \phi < \pi/2$ will yield a positive cosine term, resulting in a positive phase acceleration, and an increase in phase velocity. Electrons with phases in the range $\pi/2 < \zeta + \phi < 3\pi/2$ will yield a negative cosine term, resulting in a negative phase acceleration, and a decrease in phase velocity. At the resonance condition, electrons tend to bunch around the value of phase corresponding to zero phase velocity.

A more favorable result in terms of laser operation is found by operating above resonance, which can be achieved by injecting electrons with slightly higher energy (~1%) then would be dictated by the resonance condition. This case is depicted by Figure 6. Note that in this example, by the end of the undulator there has been more downward motion in phase space then upward motion. This means that overall, the electron pulse has transferred energy to the optical wave, resulting in a net optical gain. Also note that

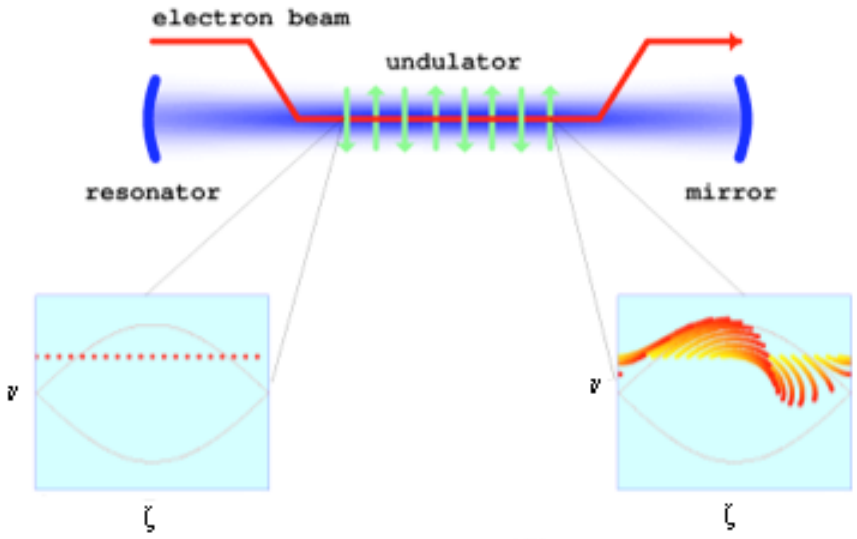

Figure 6. Phase space evolution above resonance, from [1].

the electrons are bunching around a larger phase value then they did at the resonance condition. In terms of optical gain, it is better to bunch electrons around a phase value that causes them to give up energy.

Figure 7 illustrates the idea of bunching electrons in a region that is favorable to optical gain. The red region represents values of phase corresponding to energy transfer from the optical wave to the electrons, or absorption. The green region represents values of phase corresponding to energy transfer from the electrons to the optical wave, or gain. The upper picture shows electrons at resonance, as in Figure 5. They begin at t_1 uniformly distributed in phase, and end at t_2 bunched around the phase corresponding to

zero net gain. The lower picture shows electrons above resonance, as in Figure 6. They begin at t_1 uniformly distributed in phase, and end at t_2 bunched around a higher value of phase, corresponding to positive net gain.

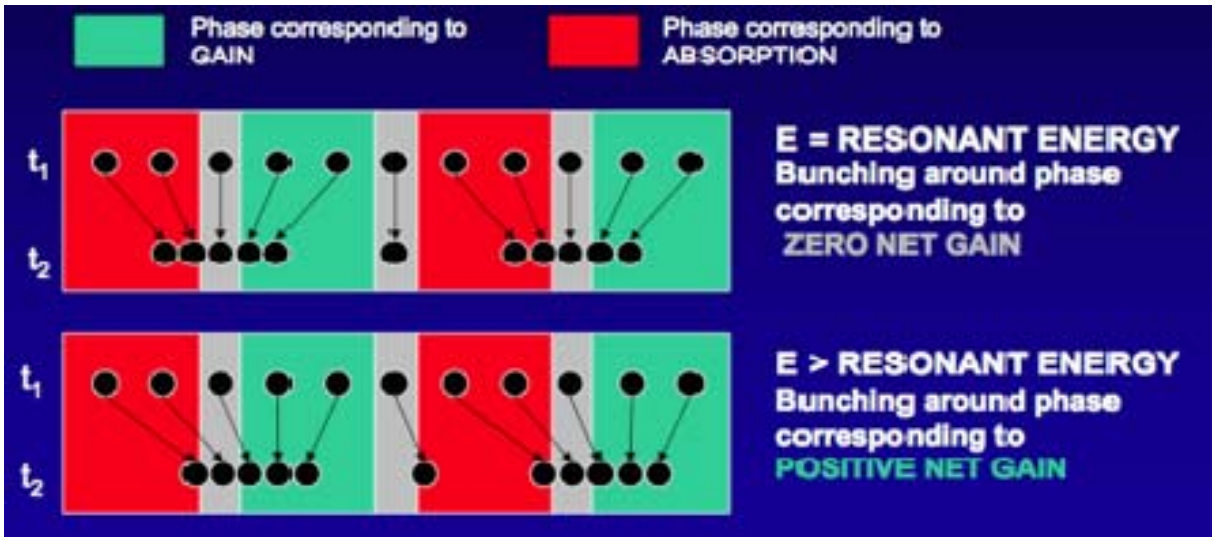

Figure 7. Proper electron bunching results in optical gain, from [23].

B. OPTICAL WAVE EQUATION

The dimensionless optical field magnitude was introduced in (4.26). The corresponding wave equation can be expressed as

$$\overset{\circ}{a} = -j < e^{-i\zeta} >, \tag{4.30}$$

where $j = 8N(e\pi KL)^2 \rho / \gamma^3 m_e c^2$ is the dimensionless electron beam current, ρ is the electron beam particle density, and $< .. >$ denotes an average over all the electrons [1]. Note that if the electrons are evenly distributed throughout phase, the average is zero. This average will only be nonzero when the electrons are bunched around a phase that has a non-zero phase velocity. Therefore, the amount by which the optical field changes depends on the electron current, and the electron bunching.

1. GAIN AND SATURATION

The optical beam gain is the fractional increase of optical field energy during one pass through the undulator, defined by

$$G = \frac{|a(\tau)|^2 - |a(0)^2|}{|a(0)^2|}. \tag{4.31}$$

From (4.27), it is clear that a strong optical field ($|a| > \pi$) is necessary for good electron bunching. Provided we have bunching at a favorable phase, (4.30) implies that the optical field will grow, leading to more bunching. The interdependence of (4.27) and (4.30) constitutes a feedback cycle that results in exponential gain.

If the optical field is too strong, however, the average electron phase can evolve to a point where the phase velocity begins to increase, which takes energy away from the optical field. This causes the gain to decrease, and the optical growth process becomes saturated. Figure 8 illustrates what this "overbunching" looks like in phase space.

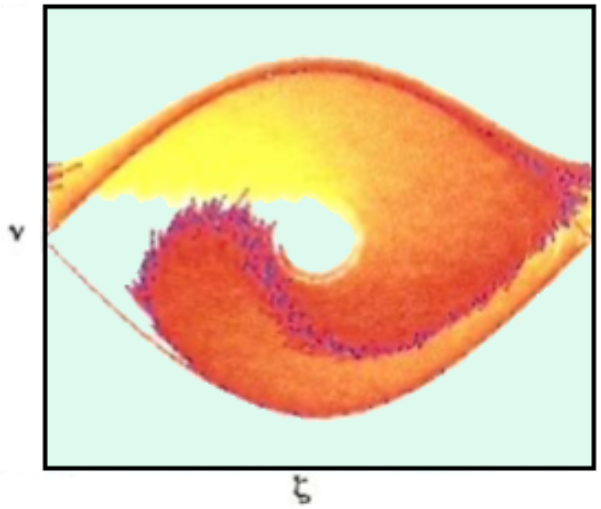

Figure 8. Overbunching, from [1]

2. Rayleigh Length Considerations

In order for a FEL to have gain, there must be overlap between the electron beam and the optical beam. To quantify this overlap, let us define the filling factor as the ratio of electron beam area to optical beam area.

Rayleigh length, Z_0, sometimes called depth of focus, is the distance from the beam waist where the beam radius has increased by a factor of $\sqrt{2}$ [26]. For a circular beam, this equates to doubling the cross sectional area of the beam. Clearly, the filling factor will depend upon the Rayleigh length.

If we assume the optical beam consists only of the fundamental Gaussian mode, then it can be shown by averaging the filling factor over the length of the undulator that the gain is [27]

$$G = \frac{G_0 / \sqrt{3}}{Z_0 / L + L / (12 Z_0)}, \tag{4.32}$$

where G_0 is the maximum gain at the optimal Rayleigh length. This expression shows that the gain will go down as the Rayleigh length gets shorter.

The shorter the Rayleigh length, the more divergent is the optical beam. If the optical beam is not sufficiently divergent, then there may be too much power concentrated in too small an area to be handled by the mirrors of the resonator cavity. As will be shown later, Rayleigh length also affects the laser's sensitivity to changes in the electron beam's trajectory.

THIS PAGE INTENTIONALLY LEFT BLANK

V. ELECTRON BEAM OPTICS

In chapter III, the electron beam transport system was mentioned along with the types of magnets commonly used in FELs. In this chapter we will examine in detail how these magnets affect the trajectory of an electron. In our calculations we will use a coordinate system that follows the electron. The direction of electron travel will be designated $\vec{s}$, while the horizontal and vertical planes are defined as $x\text{-}s$ and $y\text{-}s$ respectively. The right-hand side of Figure 9 illustrates this coordinate system, where $\vec{s}$ comes out of the page. Equation Chapter 5 Section 1

A. QUADRUPOLES

As previously stated, quadrupoles are used to focus an electron beam. Figure 9 shows a cross section of an "F" type quadrupole, which is used to focus an electron beam in the horizontal plane. "D" type quadrupoles, used to focus an electron beam in the vertical plane, are identical to the "F" type except that the poles are reversed.

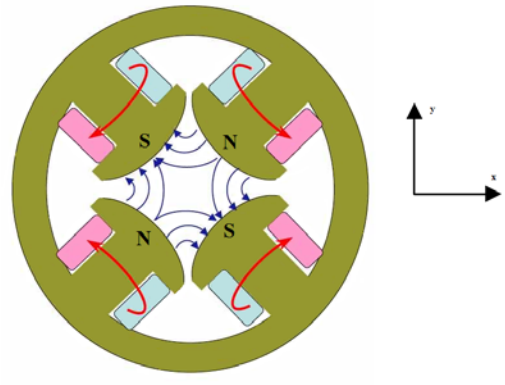

Figure 9. Cross-section of an F type quadrupole magnet, from [28].

In calculating the effect quadrupoles have on an electron's trajectory, it will be assumed that the magnetic field is constant along the s-axis, and zero outside the magnet. Results obtained through these assumptions have been shown to be in excellent agreement with measurements [5].

The Lorentz forces experienced by an electron located at (x,y), traveling in the s direction with velocity v_s, and passing through an "F" type quadrupole are

$$F_x = \gamma m_e \frac{d^2x}{dt^2} = -\frac{B|e|}{a} x v_s \tag{5.1}$$

$$F_y = \gamma m_e \frac{d^2y}{dt^2} = \frac{B|e|}{a} y v_s \tag{5.2}$$

where B is the magnetic field magnitude at the pole face and a is the semi-aperture, as shown in figure 9. Note that if x is positive, the electron experiences a force in the $-x$ direction, and vice versa. This means the quadrupole focuses in the horizontal plane. Also note that the quadrupole is defocusing in the vertical plane. If the electron is in the center of the quadrupole, no force is experienced.

It will be convenient to replace the time derivatives in (5.1) and (5.2) with derivatives with respect to s. This is possible because the electron's position in s is uniquely defined for any given time by

$$s = v_s t \approx ct ,$$

therefore

$$\frac{d^2}{dt^2} = c^2 \frac{d^2}{ds^2} . \tag{5.3}$$

Substituting (5.3) into (5.1) and (5.2) results in

$$\frac{d^2x}{ds^2} = -\kappa x , \tag{5.4}$$

$$\frac{d^2y}{ds^2} = \kappa y \tag{5.5}$$

where $\kappa = |e| B / \gamma m_e ac$ is the normalized linear field gradient. Equations (5.4) and (5.5) are second-order linear homogeneous differential equations that are easily solved analytically. Taking the initial conditions at $s = 0$ to be $x = x_0$, $y = y_0$, $dx/ds = x' = x'_0$, and $y' = y'_0$, the solutions are

$$x = x_0 \cos\left(s\sqrt{\kappa}\right) + \frac{x'_0}{\sqrt{\kappa}} \sin\left(s\sqrt{\kappa}\right), \tag{5.6}$$

$$y = y_0 \cosh\left(s\sqrt{\kappa}\right) + \frac{y'_0}{\sqrt{\kappa}} \sinh\left(s\sqrt{\kappa}\right), \tag{5.7}$$

$$x' = -x_0\sqrt{\kappa}\sin\left(s\sqrt{\kappa}\right) + x_0'\cos\left(s\sqrt{\kappa}\right), \tag{5.8}$$

$$y' = y_0\sqrt{\kappa}\sinh\left(s\sqrt{\kappa}\right) + y_0'\cosh\left(s\sqrt{\kappa}\right). \tag{5.9}$$

A more convenient way of expressing these equations is in matrix notation

$$\begin{pmatrix} x \\ x' \end{pmatrix} = \begin{pmatrix} \cos\left(s\sqrt{\kappa}\right) & \frac{1}{\sqrt{\kappa}}\sin\left(s\sqrt{\kappa}\right) \\ -\sqrt{\kappa}\sin\left(s\sqrt{\kappa}\right) & \cos\left(s\sqrt{\kappa}\right) \end{pmatrix} \begin{pmatrix} x_0 \\ x_0' \end{pmatrix}, \tag{5.10}$$

$$\begin{pmatrix} y \\ y' \end{pmatrix} = \begin{pmatrix} \cosh\left(s\sqrt{\kappa}\right) & \frac{1}{\sqrt{\kappa}}\sinh\left(s\sqrt{\kappa}\right) \\ \sqrt{\kappa}\sinh\left(s\sqrt{\kappa}\right) & \cosh\left(s\sqrt{\kappa}\right) \end{pmatrix} \begin{pmatrix} y_0 \\ y_0' \end{pmatrix}. \tag{5.11}$$

If s in (5.10) and (5.11) is taken to be the effective length of the quadrupole, then these matrices enable us to calculate the final position and trajectory of an electron whose initial position and trajectory are known [5]. For this reason, they are appropriately termed transfer matrices, analogous to what may be found in the field of optics to describe lenses. The transfer matrices for a "D" type quadrupole are the same, simply switching x with y and x' with y'.

If we wish to investigate the effect of a displaced quadrupole, we need only transform the electron to a frame where the magnet is centered, apply the transfer matrices defined above, then transform the electron back to the original reference frame. As an example,

$$\vec{x} = T\cdot(\vec{x}_0 + \vec{d}) - \vec{d}\,, \tag{5.12}$$

where T is a transfer matrix and $\vec{d}$ is the quadrupole displacement. Displaced quadrupoles alter the trajectory of the electron beam, which can effect the operation of the FEL. This will be explored in more detail later.

B. DIPOLES

Dipole magnets are used to steer the electron beam. They allow the beam to be doubled back so the overall system takes up less space. Since their only purpose is to change the direction of the electron beam, there are only two magnetic poles, yielding a

magnetic field with only one directional component. We will assume this is in the vertical plane. The relativistic Lorentz force experienced by an electron inside a dipole is

$$F_x = \gamma m_e c^2 x'' = -ev_s B_y . \tag{5.13}$$

Note that this describes the force in the laboratory frame of reference. If the electron is precisely on the s-axis with no displacement in x or y, it will remain precisely on the s-axis with no transverse displacement because of the way the s-axis is defined. We can think of dipoles as changing the path of s, the nominal path of the electron, within the laboratory reference frame. Equation (5.13) causes the s-axis to curve in the horizontal plane. The radius of curvature is found by equating the Lorentz force to a centripetal force,

$$F_R = \gamma m_e \frac{v_s^2}{R} = -ev_s B_y . \tag{5.14}$$

Solving for the radius of curvature, R, gives

$$R = -\frac{\gamma m_e v_s}{eB_y} . \tag{5.15}$$

If the electron is not precisely on the s-axis, but rather has a displacement in x, the there will be an apparent acceleration in x relative to the s-axis. In the laboratory frame, the displaced electron will have the same radius of curvature as an electron with no displacement. However, in our co-moving coordinate system, the displaced electron will move relative to the non-displaced electron. This motion can be characterized by framing the problem as a mismatch between the Lorentz force and a centripetal force with $r = R + x$.

$$\gamma m_e c^2 x'' = F_R - F_{lorentz} ,$$

$$\gamma m_e c^2 x'' = \left(\gamma m_e \frac{v_s^2}{r} \right) - \left(-ev_s B_y \right),$$

$$\gamma m_e c^2 x'' = \left(\gamma m_e \frac{v_s^2}{(R+x)} \right) + \left(ev_s B_y \right). \tag{5.16}$$

Inserting (5.15) into (5.16) and solving for x'' yields

$$x'' = -\frac{x}{R^2} \tag{5.17}$$

The solution to (5.17) expressed in matrix form is

$$\begin{pmatrix} x \\ x' \end{pmatrix} = \begin{pmatrix} \cos\left(\frac{s}{R}\right) & R\sin\left(\frac{s}{R}\right) \\ -\frac{1}{R}\sin\left(\frac{s}{R}\right) & \cos\left(\frac{s}{R}\right) \end{pmatrix} \begin{pmatrix} x_0 \\ x_0' \end{pmatrix}. \tag{5.18}$$

To obtain the transfer matrix for the vertical direction, recall that $B_x = 0$, which means $1/R = 0$. Substituting this into (5.18) gives

$$\begin{pmatrix} y \\ y' \end{pmatrix} = \begin{pmatrix} 1 & s \\ 0 & 1 \end{pmatrix} \begin{pmatrix} y_0 \\ y_0' \end{pmatrix}. \tag{5.19}$$

A transfer matrix of this form describes a drift, or region where there are no forces acting on the electron in that direction.

C. EDGES

In deriving the transfer matrices for a dipole magnet, it was once again assumed that the magnetic field was constant inside the magnet, and zero outside the magnet, just as had been done for the quadrupole. Furthermore, it was assumed that the magnetic field began and ended at the same value of s over the entire x-s plane. This is only true if the faces of the dipole are perpendicular to the s axis. This is true for sector magnets as shown in Figure 10. However, rectangular magnets are often used because they are easier to manufacture [5]. As Figure 10 shows, the face of a rectangular magnet is tilted through the angle ψ, which affects the electron's trajectory as it enters and exits the dipole.

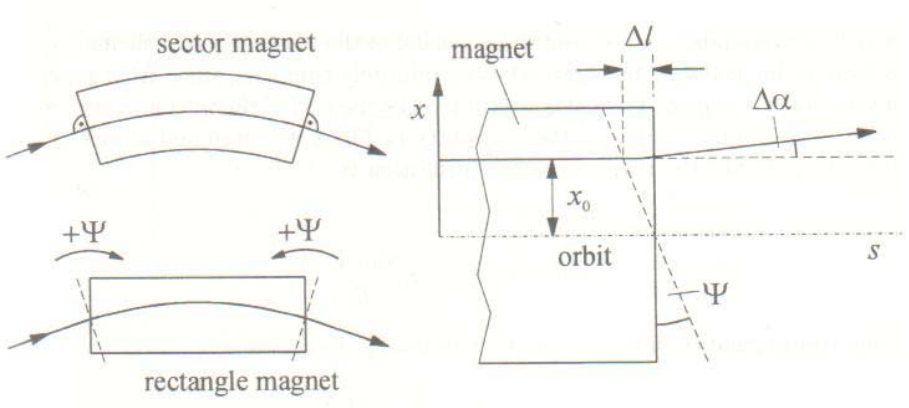

Figure 10. Sector versus rectangular magnets, from [5]

In the right hand side of Figure 10, we see that an electron with initial horizontal displacement x_0 travels a shorter distance inside the magnet than an electron with zero initial displacement. The difference in path length is

$$\Delta l = x_0 \tan\psi\,, \tag{5.20}$$

which causes the electron to be bent through a smaller angle. This difference is

$$\Delta\alpha = \frac{\Delta l}{R} = x_0 \frac{\tan\psi}{R}\,. \tag{5.21}$$

After passing through an edge, the final horizontal displacement of the electron is the same as the initial displacement, but the trajectory has been altered by $\Delta\alpha$. Hence, the transfer matrix for the edge of a rectangular dipole magnet is

$$\begin{pmatrix} x \\ x' \end{pmatrix} = \begin{pmatrix} 1 & 0 \\ \dfrac{\tan\psi}{R} & 1 \end{pmatrix} \begin{pmatrix} x_0 \\ x_0' \end{pmatrix}. \tag{5.22}$$

This implies the vertical component of the magnetic field has a gradient in the x direction. By symmetry ($\nabla \times \vec{B} = 0$), the horizontal component of the magnetic field must have a gradient in the y direction that is equal in magnitude but opposite in direction. Therefore,

$$\begin{pmatrix} y \\ y' \end{pmatrix} = \begin{pmatrix} 1 & 0 \\ -\dfrac{\tan\psi}{R} & 1 \end{pmatrix} \begin{pmatrix} y_0 \\ y_0' \end{pmatrix}. \tag{5.23}$$

VI. SIMULATIONS TO EXPLORE RAYLEIGH LENGTH DEPENDENCE OF GAIN VERSUS TILT

As mentioned in chapter IV, material considerations motivate us to develop short Rayleigh length FELs. Also as mentioned in chapter IV, decreasing the Rayleigh length can affect the on gain. Experiments at Thomas Jefferson National Accelerator Facility (TJNAF) were conducted to explore FEL performance as it relates to shift and tilt tolerances, and the affect that Rayleigh length has on these tolerances. In this section we discuss simulations that were performed for the same purpose.

To clarify our terminology, shift refers to a translation of the electron beam along either the vertical or the horizontal axis, Δx or Δy. Tilt refers to rotation of the beam about a point, $\Delta x'$ or $\Delta y'$. In aviation parlance, a vertical tilt corresponds to pitch, while a horizontal tilt corresponds to yaw. In this section all shifts and tilts are in the vertical direction, which is in the plane of the undulator field.

A. 3D FEL OSCILLATOR SIMULATIONS

The 3D FEL simulator was created by Professor Colson and Professor Blau at the Naval Postgraduate School (NPS) [29]. This code runs on a 64 node, 128 processor Apple Xserve cluster. An input file specifies parameters for the electron beam, the undulator, and the optical cavity, and the output provides information for the evaluation of laser performance, such as gain and extraction. Gain was defined in chapter IV. Extraction is the output optical power divided by the average power of the electron beam.

Table 2 summarizes the properties of the electron beam, which match the properties of the system at TJNAF. The energy of the electron beam exiting the accelerator is 111 MeV. The electron pulse rate is 4.7 MHz, with a pulse length of 0.12 mm.

ELECTRON BEAM PARAMETERS		
Eb	Beam energy (MeV)	111
qbunch	Bunch charge (nC)	0.108
rbx	Beam radius, x rms (mm)	0.2
rby	Beam radius, y rms (mm)	0.2
tb	Pulse duration, FWHM (ps)	0.4
prf	Pulse rep frequency (MHz)	4.7
lb	Pulse length, FWHM (mm)	.12
gamma	Lorentz factor	218
Ipeak	Peak current (A)	270
Iavg	Average current (mA)	0.5
emitx	Normalized rms x emittance (mm mrad)	7.5
emity	Normalized rms y emittance (mm mrad)	7.5
emitl	Longitudinal emittance (keV ps)	70
dgog	Beam energy spread (%)	0.37
dthetax	Beam angular spread, x rms (mrad)	0.17
dthetay	Beam angular spread, y rms (mrad)	0.17
rho	Beam density (1/cm^3)	2.2×10^{13}
Pb	Beam average power (MW)	0.46

Table 2. Electron Beam Parameters

The properties of the undulator are summarized in Table 3, which again were chosen to correspond with the system at TJNAF. There are 30 undulator periods, with an undulator period of 5.5 cm, to give an undulator length of 165 cm.

UNDULATOR PARAMETERS		
lambda0	Undulator period (cm)	5.5
N	Number of periods	30
gap	Undulator gap (cm)	4
Bpeak	Undulator peak magnetic field (T)	0.22
Brms	Undulator magnetic field, rms (T)	0.16
K	Undulator parameter, rms	0.81
L	Undulator length (cm)	165

Table 3. Undulator Parameters

Table 4 lists the optical cavity parameters. The optical cavity length, which is the distance between the mirrors, is 32 m. The cavity quality factor is 17, giving an output coupling of 5.9%. The optical wavelength is 0.96 microns.

OPTICAL CAVITY PARAMETERS		
S	Cavity length (m)	32
Z0	Rayleigh length (cm)	70
loss	Mirror losses per pass (%)	6
lambda	Optical wavelength (microns)	0.96
W0	Mode waist radius, 1/e (mm)	0.5
Wmir	Mode radius at mirrors, 1/e (cm)	1.1
Qn	Quality factor	17

Table 4. Optical Cavity Parameters

Table 5 lists the dimensionless parameters that are the direct inputs into the simulation. Their values are based on the physical parameters listed in Tables 2, 3, and 4.

DIMENSIONLESS PARAMETERS		
j	Normalized current density, linear undulator	20
sx	Normalized beam radius	0.28
sy	Normalized beam radius	0.28
stx	Normalized beam angular spread	0.40
sty	Normalized beam angular spread	0.40
svg	Phase velocity spread due to energy spread	1.40
sigz	Normalized pulse length	4.2
z0	Normalized Rayleigh length	0.42
w0	Normalized mode waist radius	0.65
wmir	Normalized mode radius at mirrors	15
F	Filling factor	0.51
tmir	Normalized mirror separation	19
wbeta	Betatron oscillation frequency	0.7

Table 5. Dimensionless Parameters

The simulation was used to mimic the experimental procedure followed at TJNAF wherein the electron beam was tilted, then shifted to locate the peak gain for the given value of tilt. For a given Rayleigh length, the value of tilt at which the peak gain was reduced by a factor of 2 was identified. This process was repeated for various Rayleigh lengths. In the actual laser, the Rayleigh length was controlled by attaching a heater to

one of the mirrors. The radius of curvature of the mirror, which helps determine the Rayleigh length, was proportional to the heater power. In the simulation, Rayleigh length is an input parameter that is normalized by dividing it by the undulator length.

Figure 11 displays results for some of the simulations conducted at a normalized Rayleigh length of 0.6. It will be shown that altering the Rayleigh length alters the laser's sensitivity to shifts and tilts.

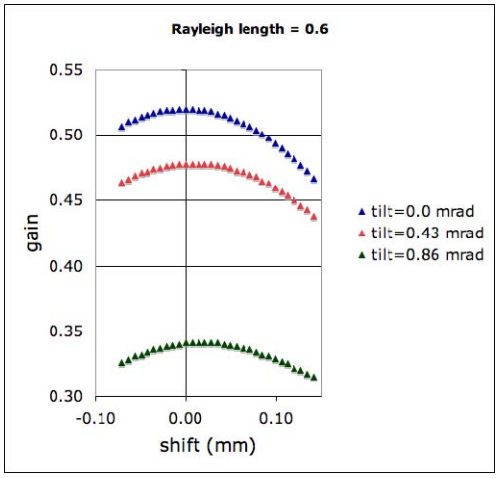

Figure 11. Gain versus shift for a normalized Rayleigh length of 0.6

From Figure 11, it would appear that the peak gain for a given tilt occurs at or very near a shift of zero. Figure 12 shows the same thing for a normalized Rayleigh length of 0.4.

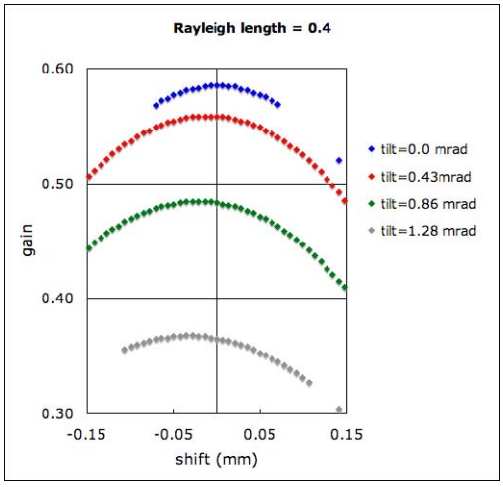

Figure 12. Gain versus shift for a normalized Rayleigh length of 0.4

While the peak gain for a given value of tilt still appears to occur very near zero shift, Figure 12 shows that this peak is drifting toward negative shift as tilt increases. This effect seems more pronounced at greater values of tilt and smaller values of Rayleigh length.

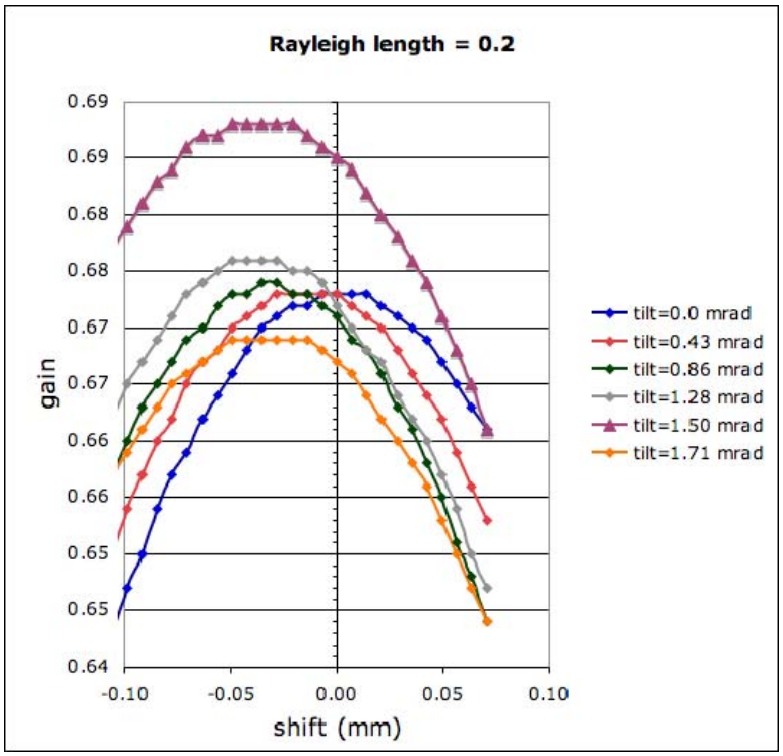

Figure 13. Gain versus shift for a normalized Rayleigh length of 0.2.

Figure 13 is the same type of plot, but for a normalized Rayleigh length of 0.2. There are two main features to note from Figure 13. First, as the tilt is increased, the peak gain goes up before going down. In Figures 11 and 12, any tilt resulted in a reduction of gain. In Figure 13, tilting the electron beam actually increased the gain. This effect is more clearly shown in Figure 14, which shows tilt versus gain for a constant shift of -.04 mm.

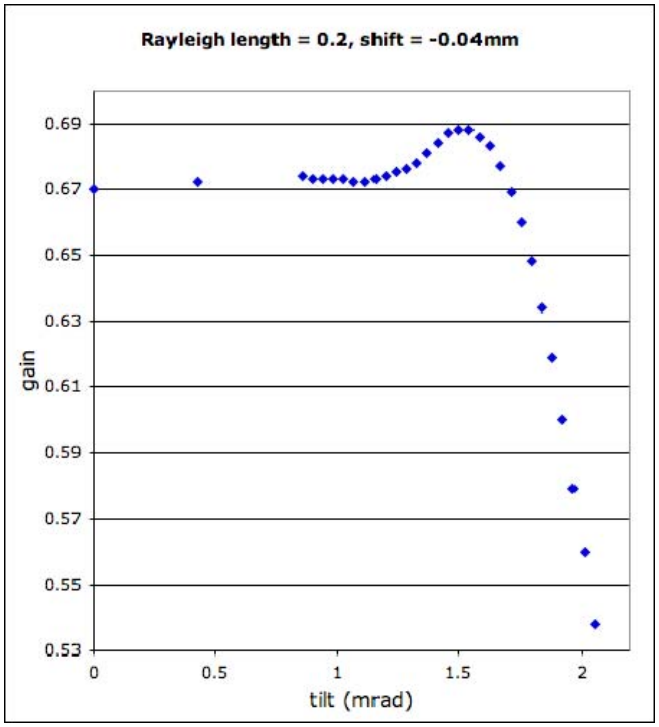

Figure 14. Gain versus tilt for a normalized Rayleigh length of 0.2.

Notice that the peak gain occurs around a tilt of 1.5 mrad. At very short Rayleigh lengths, tilting the electron beam can increase the filling factor, or overlap between the electron and optical beams. This results in a slight increase in gain. The difference between the gain at zero tilt and the gain at a tilt of 1.5 mrad is only 2%, so this is a small effect.

The second interesting feature of Figure 13 is that the peak gain for a given value of tilt clearly occurs at a negative shift. Figure 15 shows the relationship between shift and tilt with regard to the location of the peak gain. However, referring back to Figure 13 it is seen that the difference in gain between the peak value and the value at zero shift is less than 1%, so this is also a small effect.

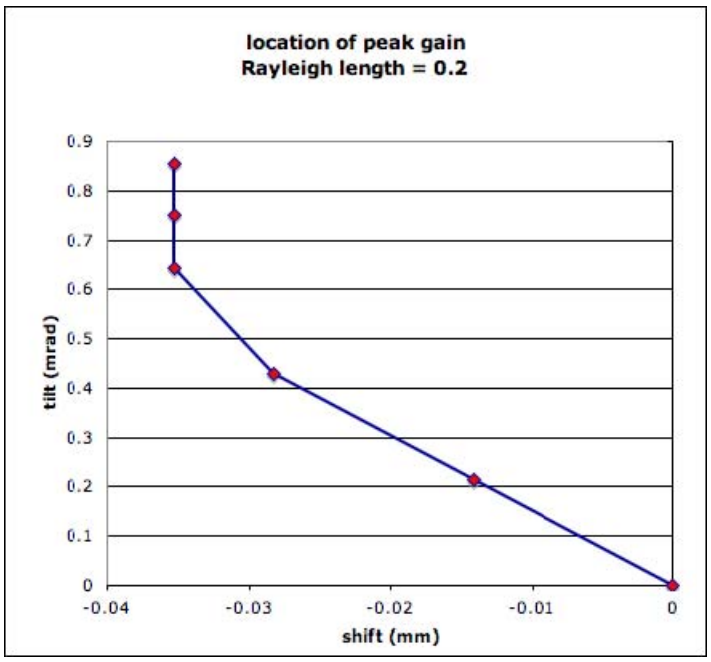

Figure 15. For a given tilt, this shows the shift at which the peak gain may be found.

An additional item of interest is seen in the trend of peak gain versus Rayleigh. Examining Figures 11, 12 and 13, it is seen that as Rayleigh length gets shorter, the peak gain goes up. This is contrary to (4.32), which does not account for electron response to the diffracting optical field [27]. Since these diffraction effects are larger at shorter Rayleigh lengths, it is not surprising that (4.32) is less accurate in this regime.

The goal of these experiments and simulations is to quantify the relationship between Rayleigh length and sensitivity to tilt. This relationship is depicted in Figure 16. For each value of normalized Rayleigh length, the value of tilt at which the gain is reduced by half (HWHM) was identified and plotted.

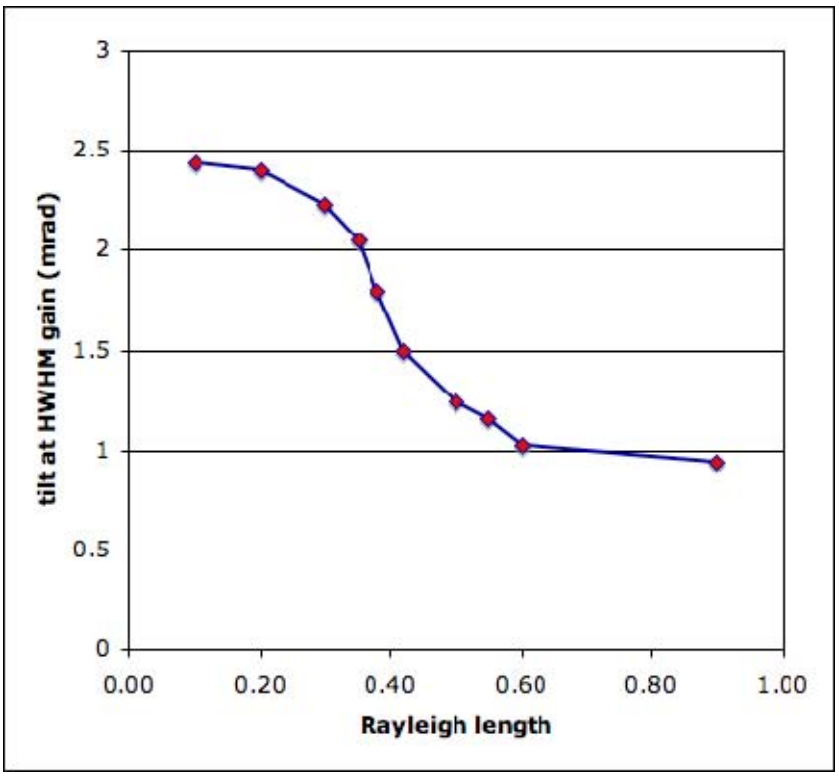

Figure 16. Dependence of a FEL's sensitivity to electron beam tilt as a function of Rayleigh Length

At longer Rayleigh lengths, the laser is more sensitive to tilting of the electron beam. At shorter Rayleigh lengths, the optical beam diverges faster, so the optical beam and the electron beam still coincide, even when the electron beam is tilted. Therefore, short Rayleigh length FELs are less sensitive to electron beam tilts.

VII. SIMULATIONS TO EXPLORE EFFECT OF QUADRUPOLE MISALIGNMENT

As explained in section V, displaced quadrupoles alter the trajectory of the electron beam. If a FEL is to be used as a shipboard weapon system, then it must operate in a vibrational environment. This series of simulations builds upon work done in a previous student thesis to establish vibration control requirements [2], and was accomplished in two stages. First, the 3D FEL oscillator simulation was used to establish maximum allowed values for horizontal and vertical shift and tilt of the electron beam. Then simulations were conducted using Trace3D and Matlab to establish peak vibration amplitudes to ensure the shift and tilt criteria are met.

A. TRACE3D AND MATLAB SIMULATIONS

Trace3D was developed at Los Alamos National Laboratory, and is an interactive beam dynamics program used to calculate the envelopes of a bunched beam as it passes through a user defined transport system [30]. The code uses transfer matrices, like those discussed in Chapter V, to produce output such as beam envelopes and phase-space ellipses. Trace3D also allows the user to specify horizontal and vertical displacements for quadrupole elements, or opt for random displacements, chosen from a uniform distribution with a user specified maximum.

Due to the user interface however, it is cumbersome to run numerous simulations in Trace3D. For this reason, the transfer matrices were copied from Trace3D and incorporated into a Matlab script. Using loops within the Matlab script, numerous simulations were run, each with its own unique set of randomly generated quadrupole displacements.

The transport system segment used in these simulations is illustrated in Figure 17. It is the same segment that was used in previous simulations of quadrupole misalignment [2], and is representative of a MW class FEL. The key elements that require calculations are quadrupoles, dipoles, and edges. The relevant design criteria for these elements are summarized in Tables 6, 7, and 8.

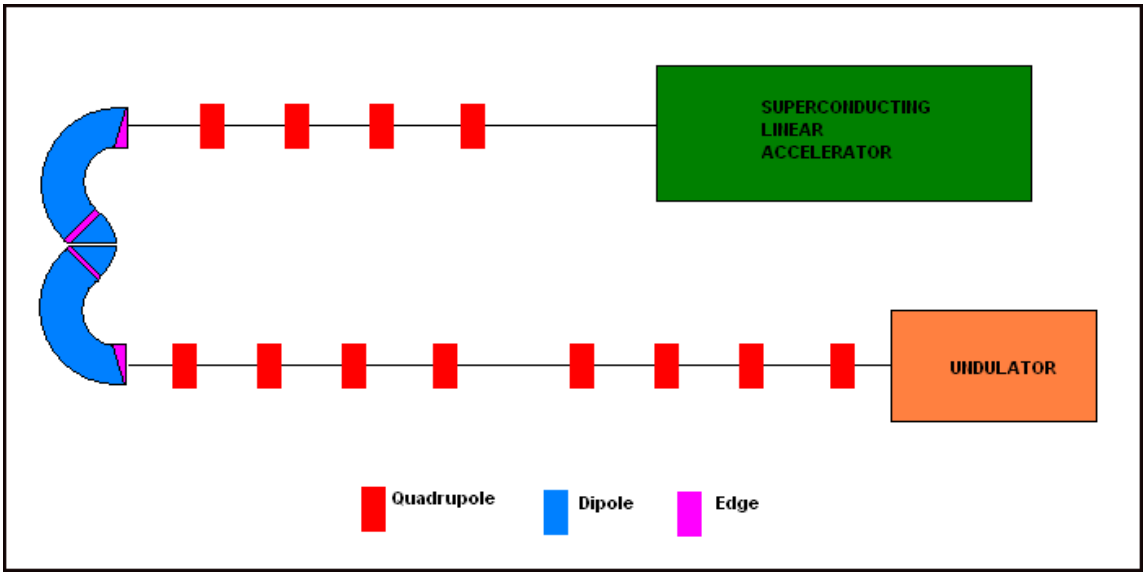

Figure 17. Segment of electron transport system, beginning at the output of the accelerator and ending at the start of the undulator.

Magnet	Gradient (T/m)	Location in z (mm)	Effective length (mm)	Beam pipe length after (mm)
Quadrupole 1	-6.19	736	150	350
Quadrupole 2	6.97	1236	150	350
Quadrupole 3	-6.16	1736	150	350
Quadrupole 4	-1.89	2236	150	175
Quadrupole 5	-11.7	5491	150	350
Quadrupole 6	0.208	5991	150	350
Quadrupole 7	-4.37	6491	150	350
Quadrupole 8	0.0004	6991	150	1706
Quadrupole 9	2.24	8847	150	350
Quadrupole 10	-2.63	9347	150	350
Quadrupole 11	3.85	9847	150	350
Quadrupole 12	-7.95	10350	150	300

Table 6. Quadrupole design criteria

The end result of introducing displacements for the quadrupoles and working through the transfer matrices is a set of four numbers describing the electron's position and trajectory. Horizontal and vertical shift are specified by x and y, while horizontal and vertical tilt are represented by x' and y'. These numbers could be entered into the FEL simulator to obtain a value of extraction. However, characterizing extraction for all possible variations of x, y, x', and y' would require tens of thousands of simulations, as well as a 5D plot. Instead, it is convenient to take advantage of the symmetry between the horizontal and vertical planes.

Magnet	Angle of bend (degrees)	Radius of curvature (mm)	Location in z (mm)
Dipole 1	-132.412	-300	2411
Dipole 2	42.412	300	3504
Dipole 3	42.412	300	3726
Dipole 4	-132.412	-300	4348

Table 7. Dipole design criteria

Magnet	Pole face rotation (degrees)	Radius of curvature (mm)	Location in z (mm)
Edge 1	45	300	2411
Edge 2	-10.075	300	3104
Edge 3	48.303	300	3504
Edge 4	48.303	300	3938
Edge 5	-10.075	300	4348
Edge 6	45	-300	5041

Table 8. Edge design criteria

B. 3D FEL SIMULATIONS

The 3D FEL simulator uses a linear undulator, which has a slight focusing effect in the horizontal plane. To achieve symmetry, the undulator pole faces are curved to provide a similar focusing effect in the vertical plane. With a high degree of symmetry, it should be possible to combine x and y into r, and x' and y' into r'. Then extraction can be used to place maximum limits on r and r'. These limits can be placed into the

Matlab script described in the previous section, and for each set of randomly generated quadrupole displacements a determination can be made as to whether or not the FEL's performance will be acceptable.

For these simulations, the input parameters were chosen to represent a MW class FEL. The parameters are summarized in Tables 9, 10, 11, and 12.

ELECTRON BEAM PARAMETERS		
Eb	Beam energy (MeV)	97.8
qbunch	Bunch charge (nC)	0.613
rbx	Beam radius, x rms (mm)	0.1
rby	Beam radius, y rms (mm)	0.1
tb	Pulse duration, FWHM (ps)	1.0
prf	Pulse rep frequency (MHz)	748.5
lb	Pulse length, FWHM (cm)	0.030
gamma	Lorentz factor	192
Ipeak	Peak current (A)	613
Iavg	Average current (mA)	459
emitx	Normalized rms x emittance (mm mrad)	2.6
emity	Normalized rms y emittance (mm mrad)	2.2
emitl	Longitudinal emittance (keV ps)	34
dgog	Beam energy spread (%)	0.08
dthetax	Beam angular spread, x rms (mrad)	0.14
dthetay	Beam angular spread, y rms (mrad)	0.11
rho	Beam density (1/cm^3)	2.1×10^{14}
Pb	Beam average power (MW)	45

Table 9. Electron Beam Parameters

UNDULATOR PARAMETERS		
lambda0	Undulator period (cm)	2.95
N	Number of periods	20
gap	Undulator gap (cm)	1
Bpeak	Undulator peak magnetic field (T)	0.88
Brms	Undulator magnetic field, rms (T)	0.62
K	Undulator parameter, rms	1.72
L	Undulator length (cm)	59

Table 10. Undulator Parameters.

OPTICAL CAVITY PARAMETERS		
S	Cavity length (m)	20
Z0	Rayleigh length (cm)	6
loss	Mirror losses per pass (%)	50
lambda	Optical wavelength (microns)	1.6
W0	Mode waist radius, 1/e (mm)	0.17
Wmir	Mode radius at mirrors, 1/e (cm)	2.9
Qn	Quality factor	2

Table 11. Optical Cavity Parameters.

DIMENSIONLESS PARAMETERS		
j	Normalized current density, linear undulator	83
sx	Normalized beam radius	0.18
sy	Normalized beam radius	0.18
stx	Normalized beam angular spread	0.15
sty	Normalized beam angular spread	0.12
svg	Phase velocity spread due to energy spread	0.21
sigz	Normalized pulse length	9.5
z0	Normalized Rayleigh length	0.1
w0	Normalized mode waist radius	0.32
wmir	Normalized mode radius at mirrors	53
F	Filling factor	0.14
tmir	Normalized mirror separation	34
wbeta	Betatron oscillation frequency	1.1

Table 12. Dimensionless Parameters.

Figure 18 shows electron beam shift versus extraction. There are two curves in the figure, one showing horizontal shift with zero vertical shift, the other showing vertical shift with zero horizontal shift. Clearly, there is a high degree of symmetry between vertical and horizontal shift.

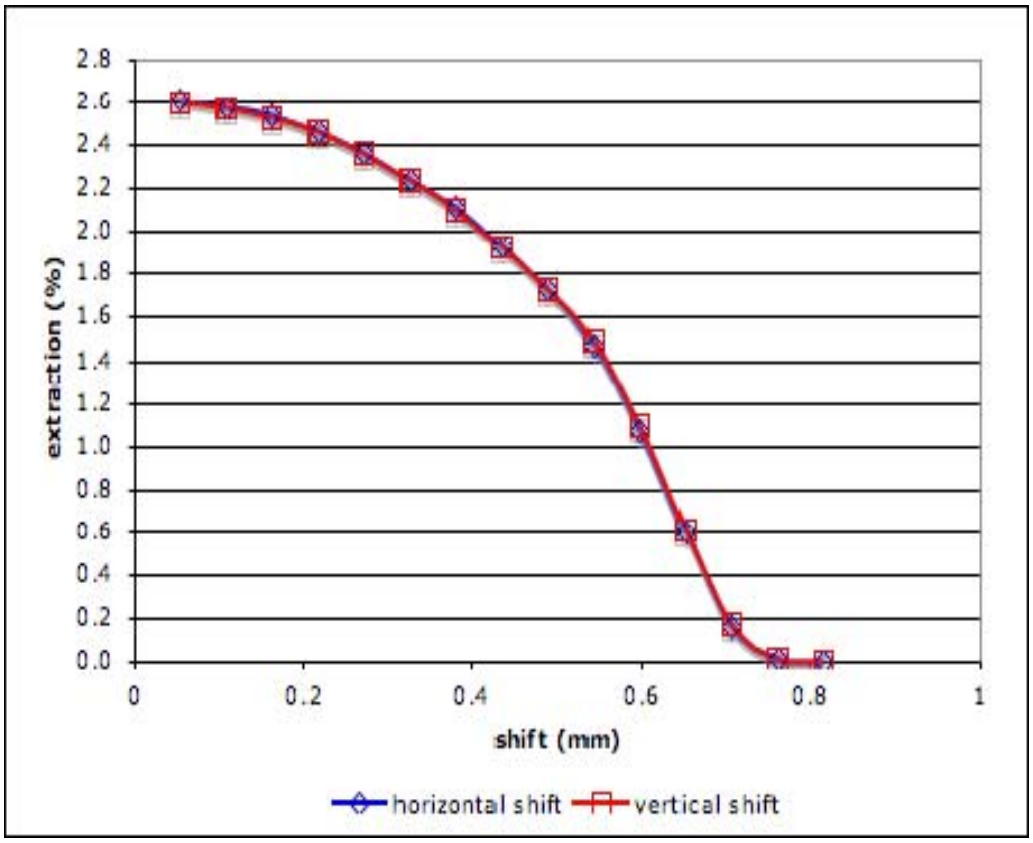

Figure 18. Shift versus extraction demonstrating symmetry between horizontal and vertical planes.

Figure 19 shows electron beam tilt versus extraction. Again, there are two curves, one showing horizontal tilt and the other showing vertical tilt, and again there is clearly a high degree of symmetry between the two planes.

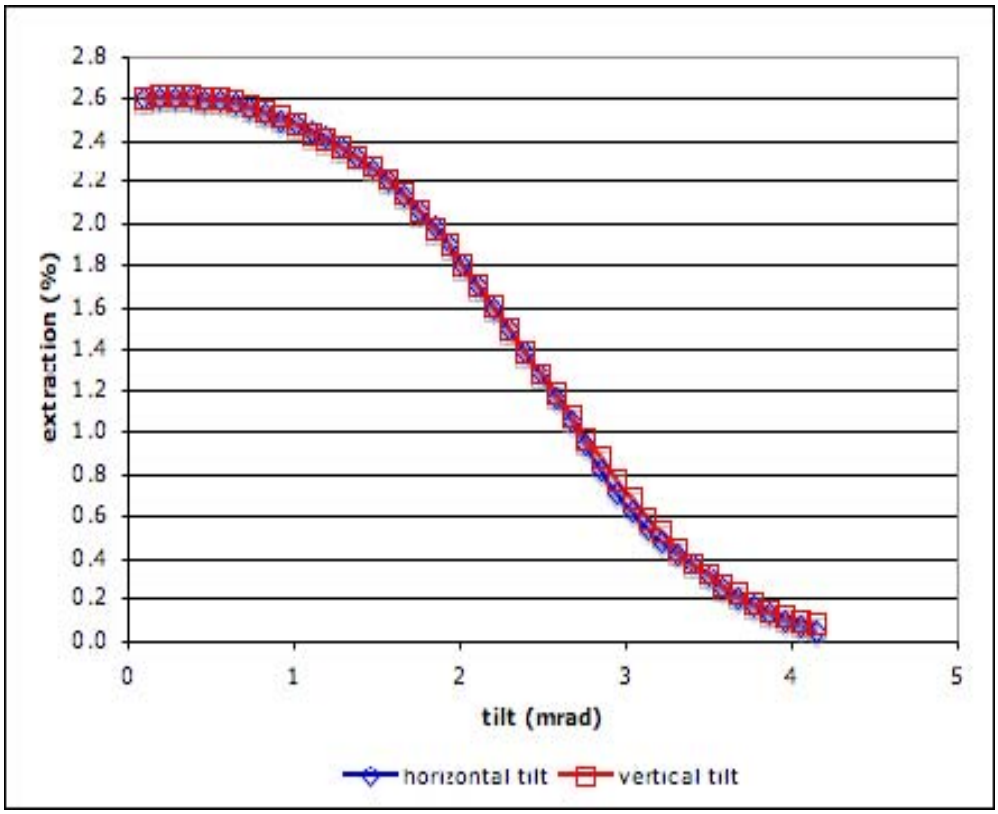

Figure 19. Tilt versus extraction demonstrating symmetry between horizontal and vertical planes.

To fully demonstrate the justification of combining x and y into r, Figure 20 shows a color-coded contour plot of extraction versus both horizontal and vertical shift. The extraction has been normalized by dividing through by the peak value, so the colorbar on right-hand side is calibrated to overall performance. A value of 1 indicates that 100% of the possible output power is realized. The radial symmetry of Figure 20 justifies the use of a single number to characterize the absolute shift off axis.

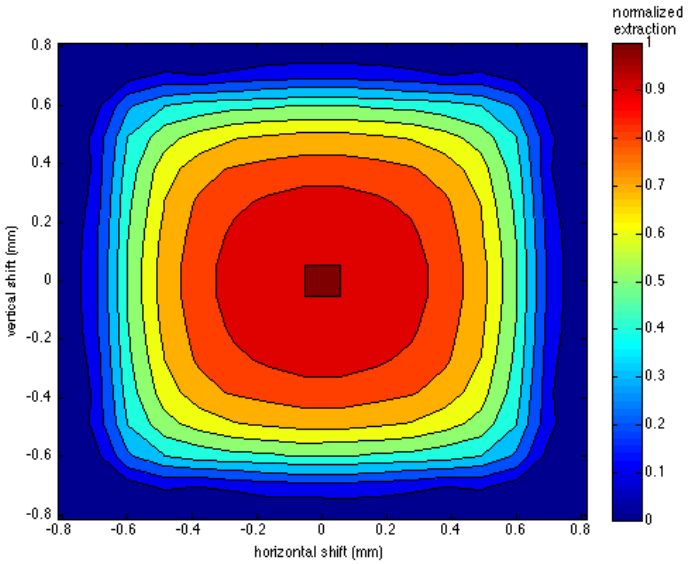

Figure 20. Normalized extraction versus horizontal and vertical shift.

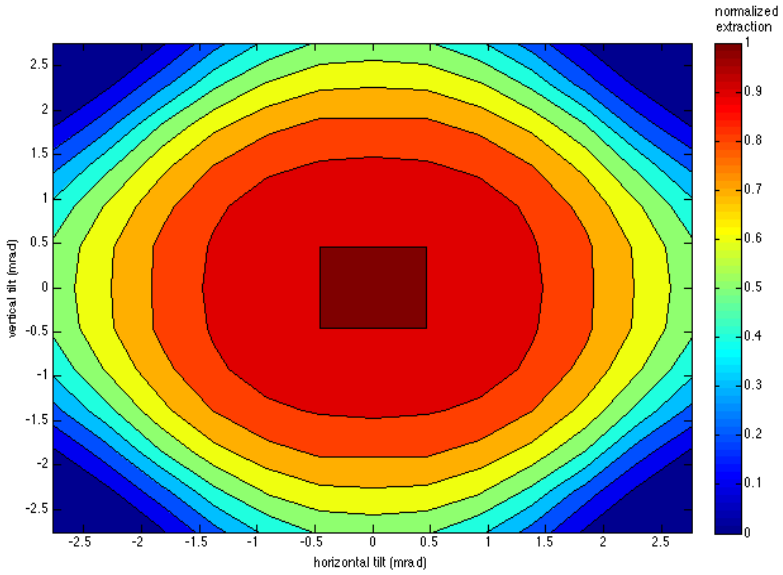

Figure 21. Normalized extraction versus horizontal and vertical tilt.

Figure 21 depicts normalized extraction versus horizontal and vertical tilt. Once again, the radial symmetry justifies combining x' and y' into r'. These combinations are made as follows:

$$r = \sqrt{x^2 + y^2}\,, \tag{5.24}$$

$$\frac{dr}{dz} = \frac{dr}{dx}\frac{dx}{dz} + \frac{dr}{dy}\frac{dy}{dz},$$

$$r' = \frac{1}{2}\left(x^2 + y^2\right)^{-1/2}(2x)x' + \frac{1}{2}\left(x^2 + y^2\right)^{-1/2}(2y)y',$$

$$r' = \left(\frac{x}{r}\right)x' + \left(\frac{y}{r}\right)y'. \tag{5.25}$$

In general, it is reasonable to consider anything more than a 20% degradation of performance unacceptable. In this case, a 20% degradation of the peak extraction, which is 2.77%, with an average electron beam energy of 45MW, results in an output optical power of < 1 MW. Therefore it is reasonable to choose cutoff values of r and r' based on a normalized extraction of 0.8. The un-normalized data for Figures 20 and 21 is presented in Tables 13 and 14. Performance of 80% of the full potential corresponds to an extraction of ~2.2%. The data in Tables 13 and 14 has been color-coded with red indicating acceptable performance and blue indicating unacceptable performance. From these tables we see it is reasonable and conservative to require $r < 0.4\,\text{mm}$ and $r' < 1.1\,\text{mrad}$.

Dimensionless		-1.3	-1.1	-0.9	-0.7	-0.5	-0.3	-0.1	0.1	0.3	0.5	0.7	0.9	1.1	1.3
	Actual (mm)	-0.7	-0.6	-0.5	-0.4	-0.3	-0.2	-0.1	0.1	0.2	0.3	0.4	0.5	0.6	0.7
-1.3	-0.7	0.0	0.1	0.3	0.3	0.3	0.4	0.4	0.4	0.4	0.3	0.3	0.3	0.1	0.0
-1.1	-0.6	0.1	0.8	1.1	1.2	1.3	1.4	1.4	1.4	1.4	1.3	1.2	1.1	0.8	0.1
-0.9	-0.5	0.3	1.1	1.6	1.8	1.9	2.0	2.0	2.0	2.0	1.9	1.8	1.6	1.1	0.3
-0.7	-0.4	0.3	1.2	1.8	2.1	2.3	2.3	2.4	2.4	2.3	2.2	2.1	1.8	1.2	0.3
-0.5	-0.3	0.3	1.3	1.9	2.3	2.4	2.5	2.6	2.6	2.5	2.4	2.3	1.9	1.3	0.3
-0.3	-0.2	0.4	1.4	2.0	2.3	2.5	2.7	2.7	2.7	2.7	2.5	2.3	2.0	1.4	0.4
-0.1	-0.1	0.4	1.4	2.0	2.4	2.6	2.7	2.8	2.8	2.7	2.6	2.4	2.0	1.4	0.4
0.1	0.1	0.4	1.4	2.0	2.4	2.6	2.7	2.8	2.8	2.7	2.6	2.4	2.0	1.4	0.4
0.3	0.2	0.4	1.4	2.0	2.3	2.5	2.7	2.7	2.7	2.7	2.5	2.3	2.0	1.4	0.4
0.5	0.3	0.3	1.3	1.9	2.3	2.4	2.5	2.6	2.6	2.5	2.4	2.3	1.9	1.3	0.3
0.7	0.4	0.3	1.2	1.8	2.1	2.3	2.3	2.4	2.4	2.3	2.2	2.1	1.8	1.2	0.3
0.9	0.5	0.3	1.1	1.6	1.8	1.9	2.0	2.0	2.0	2.0	1.9	1.8	1.5	1.1	0.3
1.1	0.6	0.1	0.8	1.1	1.2	1.3	1.4	1.4	1.4	1.4	1.3	1.2	1.1	0.8	0.1
1.3	0.7	0.0	0.1	0.3	0.3	0.3	0.4	0.4	0.4	0.4	0.3	0.3	0.3	0.1	0.0

Table 13. Extraction versus horizontal and vertical shift.

Dimensionless		-3	-2.5	-2	-1.5	-1	-0.5	0	0.5	1	1.5	2	2.5	3
	Actual (mrad)	-1.6	-1.4	-1.1	-0.8	-0.5	-0.3	0.0	0.3	0.5	0.8	1.1	1.4	1.6
-3.0	-2.76	0.0	0.0	0.2	0.7	1.2	1.4	1.5	1.4	1.2	0.7	0.2	0.0	0.0
-2.5	-1.36	0.0	0.2	0.7	1.3	1.7	1.9	1.9	1.9	1.7	1.3	0.7	0.2	0.0
-2.0	-1.09	0.2	0.7	1.4	1.9	2.1	2.3	2.3	2.3	2.1	1.9	1.4	0.7	0.2
-1.5	-0.81	0.7	1.3	1.9	2.2	2.4	2.5	2.5	2.5	2.4	2.2	1.9	1.3	0.7
-1.0	-0.54	1.2	1.7	2.1	2.4	2.6	2.7	2.7	2.7	2.6	2.4	2.1	1.7	1.2
-0.5	-0.27	1.4	1.9	2.3	2.5	2.7	2.8	2.8	2.8	2.7	2.5	2.3	1.9	1.4
0.0	0.00	1.5	1.9	2.3	2.6	2.7	2.8	2.8	2.8	2.7	2.6	2.3	1.9	1.5
0.5	0.27	1.4	1.9	2.3	2.5	2.7	2.8	2.8	2.8	2.7	2.5	2.3	1.9	1.4
1.0	0.54	1.2	1.7	2.1	2.4	2.6	2.7	2.7	2.7	2.6	2.4	2.1	1.7	1.2
1.5	0.81	0.7	1.3	1.9	2.2	2.4	2.5	2.5	2.5	2.4	2.2	1.9	1.3	0.7
2.0	1.09	0.2	0.7	1.4	1.9	2.1	2.3	2.3	2.3	2.1	1.9	1.4	0.7	0.2
2.5	1.36	0.0	0.2	0.7	1.3	1.7	1.9	1.9	1.9	1.7	1.3	0.7	0.2	0.0
3.0	1.63	0.0	0.0	0.2	0.7	1.2	1.4	1.5	1.4	1.2	0.7	0.2	0.0	0.0

Table 14. Extraction versus horizontal and vertical tilt.

Figure 22 shows the percent of the time the above criteria will be met versus the maximum allowed value of displacement, assuming a uniform distribution. Figure 23 shows the percentage versus the standard deviation of displacement, assuming a Gaussian distribution.

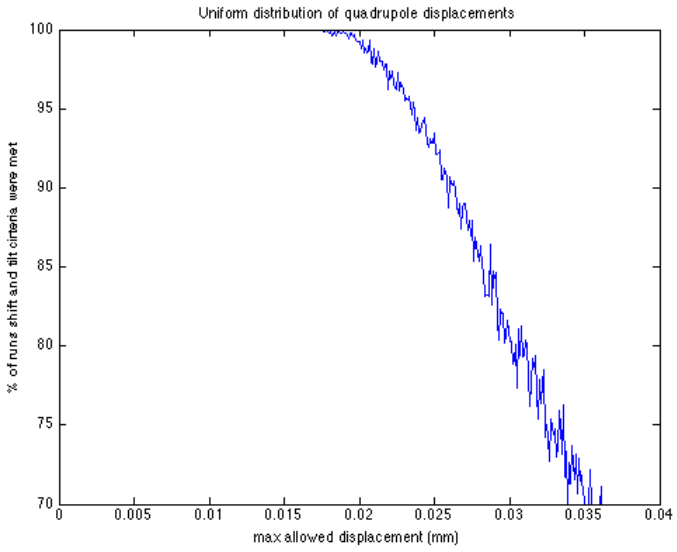

Figure 22. Reliability versus peak displacement for a uniform distribution.

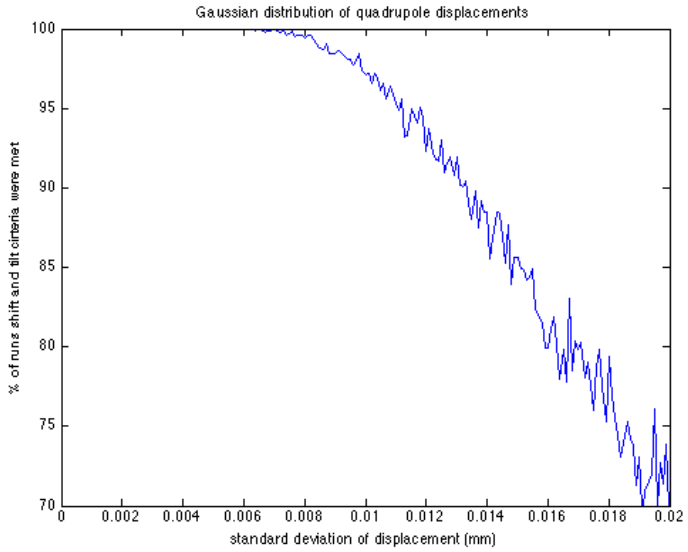

Figure 23. Reliability versus standard deviation of displacement for a Gaussian distribution.

From Figures 22 and 23 we can see that to ensure an acceptable level of optical output power 100% of the time, uniformly distributed quadrupole displacements must be kept less than ~ 0.02 mm, or 20 microns. For a Gaussian distribution of quadrupole displacements, 100% reliable requires the standard deviation to be kept less than .007 mm, or 7 microns.

THIS PAGE INTENTIONALLY LEFT BLANK

VIII. CONCLUSION

It has been shown that in order to function as a weapon system, a FEL must have an output optical power on the order of 1 MW. The performance can be reduced due to shipboard vibrations. It is has not been determined what the exact output power of the eventual weapon will be, nor is it known beyond a rough estimate how much power is required to successfully engage an incoming missile. Therefore, the acceptable amount of performance degradation can only be estimated. Using conservative estimates, it has been found that quadrupole alignment on a vibrating ship must be kept to within tolerances on the order of 10 microns. This is consistent with previous estimates, and within the capability of active alignment systems already in use [31, 32]. Such a system will be required to employ a FEL onboard a ship, but these tolerances do not comprise an insurmountable engineering problem.

THIS PAGE INTENTIONALLY LEFT BLANK

LIST OF REFERENCES

[1] William B. Colson, Class Notes, PH 4858 – Electric Ship Weapon Systems, Fall 2007.

[2] David Thomas Burggraff, "Free Electron Laser Performance with Quadrupole Magnet Misalignment From Shipboard Vibrations," Master's Thesis, Naval Postgraduate School, 2007.

[3] James C. Maxwell, *A Treatise on Electricity and Magnetism*, 3rd ed., Dover Publications, 1954.

[4] IEEE, "Albert W. Hull, 1880 -1966". [Online]. Available: http://www.ieee.org/web/aboutus/history_center/biography/hull.html [Accessed: 14 Jan 2008].

[5] Klaus Wille, *The Physics of Particle Accelerators*, Oxford University Press, 2000.

[6] Russell H. Varian, Sigurd F. Varian, "A High Frequency Oscillator and Amplifier", Journal of Applied Physics, vol. 10, no. 5, pp. 321-327, May 1939.

[7] Edwin M. McMillan, "The Synchrotron - A Proposed High Energy Particle Accelerator," Physical Review, vol. 68, issue 5-6, pp. 143-144, September 1945.

[8] International Union of Crystallography (June 1997), "Half a century of Synchrotron Radiation", [Online]. Available:, http://www.iucr.org/cww-top/his.synch50.html, [Accessed: 8 Mar 2008].

[9] F .R. Elder, A. M. Gurewitsch, R. V. Langmuir, H. C. Pollock, "Radiation from Electrons in a Synchrotron", Physical Review, vol. 71, issue 11, pp. 829-830, June 1947.

[10] D. Iwanenko, I. Pomeranchuk, “On the Maximal Energy Attainable in a Betatron,”, Physical Review, vol. 65, issue 11-12, pp. 343, June 1944.

[11] R. M. Phillips, “History of the Free Electron Laser,” *Welcome to IEEE Xplore 2.0: The History of the Free Electron Laser*, May 1990. [Online]. Available: http://ieeexplore.ieee.org:/xpls/abs_all.jsp?tp=&arnumber=110735, [Accessed: 12 Jan 2008].

[12] Elmer J. Gorn, U. S. Patent 2,591,350; April, 1952 (filed 1947).

[13] H. Motz, “Applications of the Radiation from Fast Electron Beams”, Journal of Applied Physics, vol. 22, no. 5, pp. 527-535, May 1951.

[14] H. Motz, W Thon, R. N. Whitehurst, “Experiments on Radiation by Fast Electron Beams”, Journal of Applied Physics, vol. 24, no. 7, pp. 826-833, July 1953.

[15] H. Motz, K. B. Mallory, “Generation of Submillimeter Waves”, Journal of Applied Physics, vol. 26, no. 11, November 1955.

[16] H. Motz, D. Walsh, “Dependence of Power Radiated on Beam Current in a Magnetic Undulator”, Journal of Applied Physics, vol. 33, no. 3, March 1962.

[17] R. M. Phillips, “The Ubitron, a High-Power Traveling-Wave Tube Based on a Periodic Beam Interaction in Unloaded Waveguide”, IEEE Transaction on Electron Devices, vol. 7, issue 4, pp. 231-241, October 1960.

[18] D. A. G. Deacon, L. R. Elias, J. M. J. Madey, G. J. Ramian, H. A. Schwettman, T.I. Smith, “First Operation of a Free-Electron Laser”, Physical Review Letters, vol. 38, no. 16, April 1977.

[19] Thomas Jefferson Lab National Accelerator Facility, “Free Electron Laser Program”. [Online]. Available: http://www.jlab.org/FEL/applications.html, [Accessed: 14 Jan 2008].

[20] Shiv K. Sharma, J.M.J. Madey, Eric B. Szarmes, David M. Tratt, “Remote Sensing Applications of a Free Electron Laser Lidar”, Geoscience and Remote Sensing Symposium, 2000, vol. 6, pp 2471-2473, 24-28 July 2000.

[21] Frank Carroll, “Medical Applications of the Free Electron Laser,” in *Tunable Laser Applications*, Chapter 6, F. J. Duarte, Ed., Marcel Dekker Inc., 1995.

[22] Kenneth Barbalace, “Periodic Table of Elements – Aluminum – Al EnvironmentalChemistry.com”, 1995 [Online]. Available: http://environmentalchemistry.com/yogi/periodic/Al.html#Physical, [Accessed 20 Jan 2008].

[23] N. Thompson, Introduction to Free Electron Lasers, Technical report, Accelerator Science and Technology, 2003.

[24] Gregory G. Allgaier, “The Shipboard Employment of a Free Electron Laser Weapon System,” Master’s Thesis, Naval Postgraduate School, 2003.

[25] W.B. Colson, “Classical Free Electron Laser Theory,” in *Free Electron Laser Handbook*, Chapter 5, W.B. Colson, C. Pelligrini, A. Renieri, Eds.,Elsevier Science Publishing Co., Inc., The Netherlands, 1990.

[26] William T. Silfvast, *Laser Fundamentals*, Cambridge University Press, 1996.

[27] P.P. Crooker, et. al., “The Effect of Vibrations on Short Rayleigh Length Free Electron Lasers,” January 2008, publication pending.

[28] “UCLA PBPL – Quadrupoles”, [Online]. Available: http:// pbpl.physics.ucla.edu/Research/Technologies/Magnets/Electromagnets/Quadrupoles, [Accessed 17 Mar 2008].

[29] Joseph Blau, “Multimode Simulations of Free Electron Lasers”, Dissertation, Naval Postgraduate School, 2002.

[30] K.R. Crandall, D.P. Rusthoi, “Trace 3-D Documentation,” 3rd ed., Los Alamos National Laboratory, 1997.

[31] Charles A. Allen, “Integrating the FEL on an All-Electric Ship,” Master’s Thesis, Naval Postgraduate School, 2007.

[32] Brett E. Bateman, “Experiments on Laser Beam Jitter Control with Applications to a Shipboard Free Electron Laser,” Master’s Thesis, Naval Postgraduate School, 2007.

INITIAL DISTRIBUTION LIST

1. Defense Technical Information Center
   Ft. Belvoir, Virginia

2. Dudley Knox Library
   Naval Postgraduate School
   Monterey, California

3. William B. Colson
   Naval Postgraduate School
   Monterey, California

4. Joseph Blau
   Naval Postgraduate School
   Monterey, California